NTNU
Norwegian University of
Science and Technology

Nonlinear Analysis of 3D Beams: A Comparative Study of Geometrically Exact and the Beam Elements in ABAQUS

Anders Pjaaka Torp

Civil and Environmental Engineering
Submission date: June 2017
Supervisor: Kjell Magne Mathisen, KT

Norwegian University of Science and Technology
Department of Structural Engineering

Department of Structural Engineering
Faculty of Engineering Science and Technology
NTNU- Norwegian University of Science and Technology

ACCESSIBILITY

Open

MASTER THESIS 2017

SUBJECT AREA:	DATE:	NO. OF PAGES:
Computational mechanics	June 25th 2017	62+20 (appendix)

TITLE:

Nonlinear analysis of 3D beams: A comparative study of geometrically exact and the beam elements in ABAQUS

Ikkelineære analyser av 3D bjelker: Sammenligning a geometrisk eksakte og bjelke elementene i ABAQUS

BY:

Anders Pjaaka Torp

SUMMARY:
For several decades, the finite element method (FEM) has been widely used in nonlinear analysis of three-dimensional (3D) curved beam-like structural systems, subjected to large displacements and strains. Among the numerous approaches that have been proposed, the vast majority of them have been limited to describing the beam reference geometry as a straight line. In this thesis, the geometrically exact 3D beam element, expanded by Mathisen et al. to be able to model arbitrary shaped curved geometries, has been validated and compared with the beam elements available in ABAQUS. The thesis presents the theory of the Timoshenko beam element, as well as the shear locking phenomena and it's remedies. The theory of solving nonlinear static and dynamic equilibrium equations has also been described.

RESPONSIBLE TEACHER: Prof. Kjell Magne Mathisen

SUPERVISOR(S): Prof. Kjell Magne Mathisen (NTNU)

CARRIED OUT AT: Department of Structural Engineering, NTNU.

Abstract

For several decades, the finite element method (FEM) has been widely used in nonlinear analysis of three-dimensional (3D) curved beam-like structural systems, subjected to large displacements and strains. Among the numerous approaches that have been proposed, the vast majority of them have been limited to describing the beam reference geometry as a straight line. In this thesis, the geometrically exact 3D beam element, expanded by Mathisen et al.[15] to be able to model arbitrary shaped curved geometries, has been validated and compared with the beam elements available in ABAQUS. The thesis presents the theory of the Timoshenko beam element, as well as the shear locking phenomena and it's remedies. The theory of solving nonlinear static and dynamic equilibrium equations has also been described.

Sammendrag

I flere tiår har elementmetoden (FEM) blitt brukt til å simulere tredimensjonale, kurvede bjelkelignende strukturer, utsatt for store forskyvninger og tøyninger. Av de mange metodene som er blitt presentert de siste tiårene, har flertallet av dem ikke vært i stand til å beskrive bjelker med andre referansegeometrier enn rette linjer. I denne masteroppgaven er det geometrisk eksakte bjelkeelementet, utvidet av Mathisen et al.[15] til å kunne representere vilkårlig kurvede referansegeometrier, blitt validert og sammenlignet med bjelkeelementene som er tilgjengelig i ABAQUS. Masteroppgaven presenterer teorien for Timoshenko bjelkeelementer og forklarer fenomenet shear locking, og hvordan man kan eliminere dette fra bjelkeelementet. Løsningen på ikke-lineære likevektsligninger for statiske og dynamiske problemer blir også presentert.

Preface

This master thesis has been written as part of the Master's Program at the Norwegian University of Science and Technology (NTNU), Department of Structural Engineering in the spring of 2017.

I would like to thank my advisor prof. Kjell Magne Mathisen for his guidance throughout the process.

Trondheim, June 2017

Anders Pjaaka Torp

Contents

Abstract **i**

Sammendrag **iii**

Preface **v**

1 Introduction **1**

2 Timoshenko beam element **3**

2.1 Discretization of the displacement field 10

2.2 Shear locking 14

2.3 Reduced integration 18

2.4 Residual bending flexibility, RBF 19

3 Nonlinear Equilibrium Equations **21**

3.1 Solving Nonlinear Equilibrium Equations 23

3.2 Nonlinear Dynamic Equilibrium Equations 26

3.3 Strain measures for large deformations 31

4 Numeric results **37**

4.1 Three legged beam 40
4.2 Curved beam 43
4.3 Dynamic 47

5 Summary and Conclusion **57**

A IFEM Input Files **63**

Dynamic **65**

Three Legged Beam **69**

Curved Beam **73**

B ABAQUS Input FIles **77**

Dynamic **79**

Three Legged Beam **83**

Curved Beam **87**

List of Figures

2.1 The shear distribution in a Timoshenko beam compared with the exact distribution 7
2.2 Shear parameters for different geometries 8

3.1 Algorithm describing the full Newton-Rahpson 25
3.2 Geometry description for large deformations in a Cartesian coordinate system 31
3.3 Geometry description for large deformations for the GE beam model 33

4.1 Displacement versus applied load for the Three legged beam . 38
4.2 Geometry, properties and loading of the three legged beam . . 40
4.3 Displacement and rotation plot for the 2-noded elements for the three legged beam 41
4.4 Displacement and rotation plot for the higher order elements for the three legged beam 42
4.5 Displacement and rotation plot for all the elements for the three legged beam 42
4.6 Geometry, loading and the beam properties of the curved beam 43

4.7 Displacement and rotation plot for the 2-noded elements for the curved beam 44
4.8 Displacement and rotation plot for the higher order elements for the curved beam 45
4.9 Displacement and rotation plot for all the elements for the curved beam 46
4.10 Displacement plot for all the elements for the curved beam, included the internal nodes 46
4.11 Geometry, loading and beam properties for the cantilever subjected to dynamic loading 47
4.12 Displacement plot for the 2-noded GE elements 48
4.13 Velocity plot for the 2-noded GE elements 49
4.14 Acceleration plot for the 2-noded GE elements 49
4.15 Displacement plot for the RBF enhanced elements 50
4.16 Velocity plot for the RBF enhanced elements 50
4.17 Acceleration plot for the RBF enhanced elements 51
4.18 Displacement plot for the ABAQUS Euler-Bernoulli and 2-noded Timoshenko element 52
4.19 Velocity plot for the ABAQUS Euler-Bernoulli and 2-noded Timoshenko element 52
4.20 Acceleration plot for the ABAQUS Euler-Bernoulli and 2-noded Timoshenko element 53
4.21 Displacement plot for the quadratic elements 54
4.22 Velocity plot for the quadratic elements 54
4.23 Acceleration plot for the quadratic elements 55

4.24 Velocity plot for the quadratic and cubic GE elements 55

4.25 Acceleration plot for the quadratic and cubic GE elements . . 56

List of Tables

2.1 Comparison of assumptions for the Euler-Bernoulli and Timoshenko elements 4

4.1 Number of nodes and elements needed for the different elements 48

Chapter 1

Introduction

For several decades, the finite element method has been widely used in nonlinear analysis of three-dimensional (3D) curved beam-like structural systems, subjected to large displacements and strains. Among the numerous approaches that have been proposed, the vast majority of them have been limited to describing the beam reference geometry as a straight line. Mathisen *et al.*[15] has extended the geometrically exact (GE) beam model, based on Reissner's 3D beam theory [1], to model arbitrary shaped curved beam geometry. In [15], various remedies to avoid locking in Timoshenko beam elements are presented and validated for arbitrary order of interpolation of GE 3D beam elements, for the analysis of geometrically nonlinear finite deformation curved beam-like structural systems.

The purpose of this master thesis is to provide a review of the GE beam model presented in [15] for static and dynamic analysis of beam-like 3D structural problems, for both formulation and usage. The study presents theory and computational formulation, and validates the elements on non-

linear static and dynamic benchmark problems. The validation demonstrates how the geometrically exact beam elements available in IFEM compares to the nonlinear beam elements available in ABAQUS[9].

The master thesis is outlined as follows. Chapter 2 describes the Timoshenko beam element[17] and compares it to the Euler-Bernoulli element[18], before describing the shear locking effect and remedies to eliminate it. Chapter 3 describes how nonlinear equilibrium equations can be solved, both for static and dynamic problems. It also describes the two strain measures that is utilized by IFEM and ABAQUS in the numeric benchmark problems in Chapter 4. Chapter 4 presents the results from three nonlinear benchmark problems, two static and one dynamic, using the beam elements from IFEM and ABAQUS. Chapter 5 gives a summary and a conclusion to the numerical problems.

Chapter 2

Timoshenko beam element

When modelling beams, one would normally chose between two theories, the Euler-Bernoulli and the Timoshenko beam theory. Both theories are widely used within Finite Element Analysis when modelling beams. The theories excel within certain problems, but also have their restrictions. The focus in this paper is the Timoshenko theory, and as a consequence, the Euler-Bernoulli theory will only be briefly elaborated. Throughout this chapter the advantages and disadvantages of the two theories will be explained and compared, as well as countermeasures for some of their flaws. Both theories simplify the physics by assumptions. The assumptions are listed in Table 2.1[17].

The only difference in assumptions between the two theories is the last one, as shear strain is included in the Timoshenko theory, the plane sections are now no longer guaranteed to remain orthogonal to the beam axis after deformation. Excluding shear strain is a valid assumption for slender beams.

Euler-Bernoulli	Timoshenko
The vertical displacements are small and equal to the deflection of the beam axis	The vertical displacements are small and equal to the deflection of the beam axis
The lateral displacements are zero	The lateral displacements are zero
Plane sections normal to the beam axis remain plane and orthogonal to the beam axis after deformation	Plane sections remain plane after deformation

Table 2.1: Comparison of assumptions for the Euler-Bernoulli and Timoshenko elements

In order to classify beams as slender or thick, the slenderness ratio, $\lambda = \frac{L}{h}$, is introduced. When applying the Euler-Bernoulli theory on beams with $\lambda > 10$, the solution is considered to be "exact". The Timoshenko theory picks up where the Euler-Bernoulli theory falls short. By including the effect of the shear deformations, the Timoshenko beam theory is able to represent thicker beams, but at a cost. The formulation has shortcomings that introduce the problem of locking. Locking is a numerical phenomenon that gives the beam an unphysical stiffness due to an ill-conditioned equation system. In the Timoshenko beam theory, shear locking occurs when the slenderness of the beam approaches the limits of the Euler-Bernoulli theory and the Timoshenko element is not able to reproduce the same results. To unveil why this happens, it is fruitful to look into the formulation of the two theories. In the Euler-Bernoulli theory we impose zero shear strain in the element. As a consequence of this, the following relation can be written[18]:

$$\gamma_{xz} = \frac{dw}{dx} - \theta = 0 \Rightarrow \frac{dw}{dx} = \theta \tag{2.1}$$

This relation impacts how the bending strain can be written:

$$\kappa = \frac{d\theta}{dx} = \frac{d^2w}{dx^2} \tag{2.2}$$

Now both the bending and displacement strains are dependent on the deflection, which brings both advantages and disadvantages. The obvious advantage is that the number of unknowns are reduced, simplifying the equation system. The disadvantage is the demand of an increased continuity of the displacement field, as it has to be differentiated twice to reach the bending strain. This leads to the following expression for the Principal of Virtual Work (PVW)[18]:

$$\iiint \delta\epsilon_x \sigma_x \, dV = \int (\delta w f_z + \delta \frac{dw}{dx} m) \, dx + \sum_i \delta P_{zi} + \sum_j \delta (\frac{dw}{dx})_j M_j \tag{2.3}$$

Introducing the kinematic relations and manipulating the expression, the internal energy can be written as:

$$\begin{aligned}
&\varepsilon_x = \frac{du}{dw} = -z\frac{d^2w}{dx^2}, \quad \sigma_x = E\varepsilon_x = -zE\frac{d^2w}{dx^2} \\
&M = -\iiint \sigma_x z \, dA = \iiint z^2 E \frac{d^2w}{dx^2} \, dA = E\kappa \iiint z^2 \, dA = EI_y\kappa \\
&\iiint \delta\left(-z\frac{d^2w}{dx^2}\right)\left(-zE\frac{d^2w}{dx^2}\right) dV = \iiint z^2 \delta\left(\frac{d^2w}{dx^2}\right) E\frac{d^2w}{dx^2} \, dV \\
&= \int_0^L \delta\left(\frac{d^2w}{dx^2}\right) E\frac{d^2w}{dx^2} \, dx \iint z^2 \, dA = \int_0^L \delta\kappa E I_y \kappa \, dx = \int_0^L \delta\kappa M \, dx
\end{aligned} \tag{2.4}$$

In a Timoshenko beam element the same trick is not applicable as the shear strain is now included. The rotation of the cross section can now be expressed as:$\frac{dw}{dx} + \phi = \theta$, with ϕ being the additional rotation of the cross section due to shear. This changes the formulation of PVW[17]:

$$\iiint (\delta\varepsilon_x\sigma_x + \delta\gamma_{xz}\tau_{xz})\, dV = \int_0^L (\delta w f_z + \delta\theta m\, dx + \sum_i \delta w_i P_{zi} + \sum_j \delta\theta_j M_j \tag{2.5}$$

This time the formulation contains two unknowns and another contribution from the internal forces. This will in turn affect the stiffness matrix, which is shown in Section 2.2. The internal energy can once again be rewritten when the kinematic relations are included:

$$\kappa = \frac{d\theta}{dx}, \;\; \varepsilon_x = \frac{du}{dx} = -z\frac{d\theta}{dx}, \;\; \sigma_x = E\varepsilon_x = -zE\frac{d\theta}{dx} \tag{2.6}$$

$$\gamma_{xz} = \frac{dw}{dx} + \frac{du}{dx} = \frac{dw}{dx} - \theta, \;\; \tau_{xz} = G\gamma_{xz} = G(\frac{dw}{dx} - \theta) \tag{2.7}$$

$$M = -\iint \sigma_x z\, dA = E\kappa \iint z^2\, dA = EI_y\kappa \tag{2.8}$$

$$Q = \iint \tau_{xz}\, dA = \iint G\gamma_{xz}\, dA = \frac{E}{2(1+\nu)}(\frac{dw}{dx} - \theta) \iint dA = GA\gamma_{xz} \tag{2.9}$$

Equation 2.7 suggests that the shear distribution is constant throughout the height of the beam. This is known to be false, and is a flaw introduced by the assumption number three for the Timoshenko beam element in Table 2.1. In

reality the cross-section would not remain plane, but distorted as illustrated in Figure 2.1:

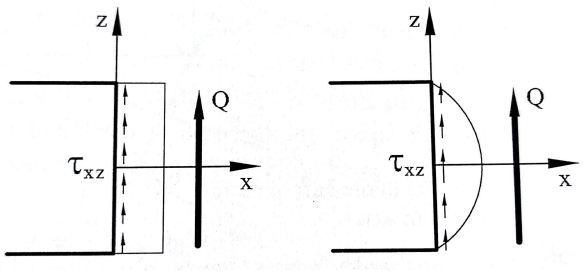

Figure 2.1: The shear distribution in a Timoshenko beam on the left, compared with the exact distribution on the right[17]

To account for this, the shear correction parameter k_z is used to reduce the cross-sectional area from A to A^*. By reducing the cross-section area the internal energy from the constant shear stress now coincides with the exact shear stress from beam theory for the PVW. To find the k_z, cylindrical bending is assumed($_{xy} = 0$) and the strain energy from the exact solution and the Timoshenko solution is compared:

$$U_s = \frac{1}{2}\iint \frac{\tau_{xz}^2}{G} dA, \quad U_s^T = \frac{Q^2}{2k_z GA} \tag{2.10}$$

Forcing the energies to be equal, the k_z can be found:

$$k_z = \frac{Q^2}{GA\iint \frac{\tau_{xz}^2}{G} dA} \tag{2.11}$$

The k_z for common cross-sections can be found in tables, some examples are given in Figure 2.2:

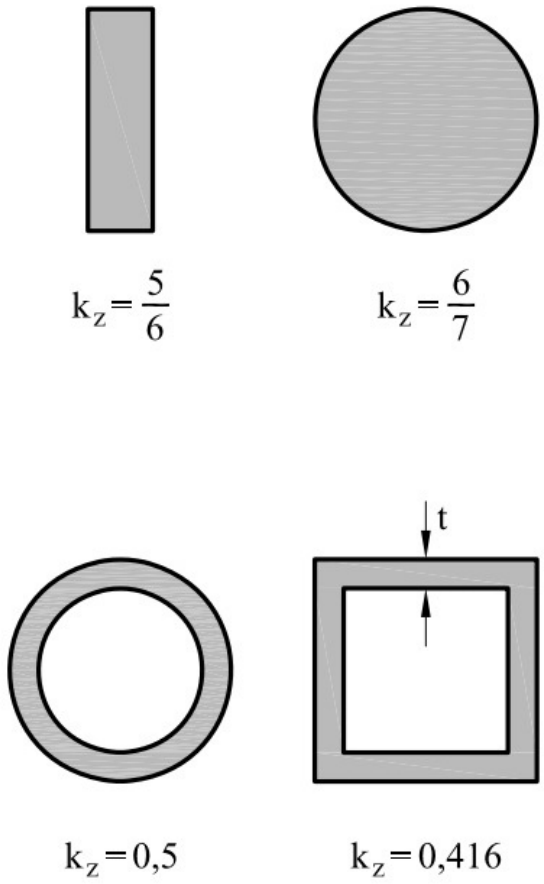

Figure 2.2: Shear parameters for different geometries[17]

Now the strains can be introduced to the PVW formulation:

$$\iiint (\delta\varepsilon_x\sigma_x + \delta_{xz}\tau_{xz}dV$$
$$= \iiint \left(\delta\left(\frac{d\theta}{dx}\right)\left(-\iint z\sigma_x dA\right) + \delta\left(\frac{dw}{dx} - \theta\right)\left(\iint \tau_{xz}dA\right)dx$$
$$= \int \left(\frac{d\theta}{dx}M + \delta\gamma_{xz}Q\right)dx \quad (2.12)$$

The PVW formulation is written for both the Euler-Bernoulli theory in Equation 2.13 and the Timoshenko theory in Equation 2.14:

$$\int \delta\kappa M dx = \int \left(\delta w f_z + \delta\left(\frac{dw}{dx}\right)m\right)dx + \sum_i \delta w_i P_{zi} + \sum_j \delta\left(\frac{dw}{dx}\right)_j M_j \quad (2.13)$$

$$\int \left(\delta\left(\frac{d\theta}{dx}\right)M + \delta\gamma_{xz}Q\right)dx = \int (\delta w f_z + \delta\theta m)dx + \sum_i \delta w_i P_{zi} + \sum_j \delta\left(\frac{dw}{dx}\right)_j M_j \quad (2.14)$$

Comparing the two expressions, the following differences is notable:

- The rotations of the cross-section and the displacements are coupled in Euler-Bernoulli theory, but not in Timoshenko theory.
- The Euler-Bernoulli theory demands a higher continuity of the displacement field.
- The Timoshenko has an additional contribution to the internal energy.

How these differences influences the behaviour of the two elements is so

far not obvious, but will become clearer in the following sections when the stiffness matrices are assembled.

2.1 Discretization of the displacement field

Before the stiffness matrix can be assembled, the displacement and rotation field has to be discretized going from an infinite to a finite solution space. With FEA this is done with the help of shape functions that interpolate the displacements and rotations between the nodes[17].

$$w(\xi) = \sum_i N_i(\xi) w_i \tag{2.15}$$

$$\theta(\xi) = \sum_i N_i(\xi) \theta_i \tag{2.16}$$

$$\mathbf{u} = \{w(\xi)\ \theta(\xi)\}^T \tag{2.17}$$

Further the strains are discretized:

$$\kappa = \frac{d\theta}{dx} = \frac{d\xi}{dx}\frac{d\theta}{d\xi} = \frac{d\xi}{dx}\left(\sum_i \frac{dN_i}{d\xi_i}\theta_i\right) \tag{2.18}$$

$$\gamma_{xz} = \frac{dw}{dx} = \frac{d\xi}{dx}\left(\sum_i \frac{dN_i}{d\xi}\theta\right) - \left(\sum_i N_i\theta_i\right) \tag{2.19}$$

and in matrix notation:

$$\kappa = \mathbf{B}_b\mathbf{a}^{(e)}, \quad \gamma_{xz} = \mathbf{B}_s\mathbf{a}^{(e)} \tag{2.20}$$

With $\mathbf{a}^{(e)}$ being the nodal displacement vector. For a simple 2-noded element with linear shape functions N_1 and N_2, $\mathbf{a}^{(e)}$, $\mathbf{B}_s$ and $\mathbf{B}_b$ can be deduced:

$$\mathbf{a}^{(e)} = \{w_1 \ \theta_1 \ w_2 \ \theta_2\}^T \tag{2.21}$$

The element utilizes the *isoparametric concept*, thus the geometry is also interpolated by the shape functions:

$$x = \sum_{i=1}^{2} N_i(\xi) x_i = \frac{1}{2}(1-\xi)x_1 + \frac{1}{2}(1+\xi)x_2 \tag{2.22}$$

From this expression $\frac{dx}{d\xi}$ is deduced, which in turns gives $\frac{d\xi}{dx}$:

$$\frac{dx}{d\xi} = \frac{1}{2}x_1 + \frac{1}{2}x_2 = \frac{l^{(e)}}{2} \Rightarrow \frac{d\xi}{dx} = \frac{2}{l^{(e)}} \tag{2.23}$$

Inserted in the $\mathbf{B}$ matrices yields:

$$\mathbf{B}_s = \begin{bmatrix} 0 & \frac{d\xi}{dx}\frac{dN_1}{d\xi} & 0 & \frac{d\xi}{dx}\frac{dN_2}{d\xi} \end{bmatrix} = \begin{bmatrix} 0 & -\frac{1}{l^{(e)}} & 0 & \frac{1}{l^{(e)}} \end{bmatrix} \tag{2.24}$$

$$\mathbf{B}_s = \begin{bmatrix} \frac{d\xi}{dx}\frac{dN_1}{d\xi} & -N_1 & \frac{d\xi}{dx}\frac{dN_2}{d\xi} & -N_2 \end{bmatrix} = \begin{bmatrix} -\frac{1}{l^{(e)}} & \frac{-(1-\xi)}{2} & \frac{1}{l^{(e)}} & \frac{-(1+\xi)}{2} \end{bmatrix} \tag{2.25}$$

Inserted in the PVW expression:

$$\int_0^L (\delta\kappa M + \delta\gamma_{xz} Q) = \int_0^L (\delta w f_z + \delta\theta m)dx + \sum_i \delta w_i P_{zi} + \sum_j \delta\theta M_j \tag{2.26}$$

$$= \int_0^L (\delta\kappa EI_y + \delta\gamma_{xz} GA^* \gamma_{xz}) dx = \int_0^L \delta \mathbf{u}^T \begin{Bmatrix} f_z \\ m \end{Bmatrix} dx + \delta \mathbf{a}^{(e)T} \mathbf{q}^{(e)} \tag{2.27}$$

$$= \int_0^L (\delta(\mathbf{B}_b^T \mathbf{a}^{(e)}) EI_y \mathbf{B}_b \mathbf{a}^{(e)} + \delta(\mathbf{B}_s^T \mathbf{a}^{(e)}) GA^* \mathbf{B}_s \mathbf{a}^{(e)}) dx = \int_0^L \delta \mathbf{N}^T \mathbf{a}^{(e)}) \begin{Bmatrix} f_z \\ m \end{Bmatrix} dx + \delta \mathbf{a}^{(e)T} \mathbf{q}^{(e)} \tag{2.28}$$

With

$$\mathbf{N}_i = \begin{bmatrix} N_1 & 0 \\ 0 & N_2 \end{bmatrix}, \quad \mathbf{N}^T = \begin{Bmatrix} \mathbf{N}_1 & \mathbf{N}_2 \end{Bmatrix}, \quad \mathbf{q}^{(e)} = \begin{Bmatrix} F_{z1} & M_1 & F_{z2} & M_2 \end{Bmatrix} \tag{2.29}$$

$$= \int_0^L (\mathbf{B}_b^T EI_y \mathbf{B}_b + \mathbf{B}_s^T GA^* \mathbf{B}_s) \delta \mathbf{a}^{(e)} \mathbf{a}^{(e)} dx = \int_0^L \mathbf{N}^T \begin{Bmatrix} f_z \\ m \end{Bmatrix} \delta \mathbf{a}^{(e)} dx + \delta \mathbf{a}^{(e)T} \mathbf{q}^{(e)} \tag{2.30}$$

$$\mathbf{a}^{(e)} \int_0^L (\mathbf{B}_b^T EI_y \mathbf{B}_b + \mathbf{B}_s^T GA^* \mathbf{B}_s) dx - \int_0^L \mathbf{N}^T \begin{Bmatrix} f_z \\ m \end{Bmatrix} dx = \mathbf{q}^{(e)} \tag{2.31}$$

Recalling Equation 2.23, the integrals can be expressed in natural coordinates:

$$dx = \frac{l^{(e)}}{2} d\xi \tag{2.32}$$

:

$$\mathbf{K}_b = \int_{-1}^{1} \mathbf{B}_b^T EI_y \mathbf{B}_b d\xi \tag{2.33}$$

$$\mathbf{K}_s = \int_{-1}^{1} \mathbf{B}_s^T GA^* \mathbf{B}_s d\xi \tag{2.34}$$

$$\mathbf{f}^{(e)} = \int_{-1}^{1} \mathbf{N}^T \begin{Bmatrix} f_z \\ m \end{Bmatrix} \frac{l^{(e)}}{2} d\xi \tag{2.35}$$

For uniformly distributed values of f_z and m the *equivalent nodal force vector*, $\mathbf{f}^{(e)}$, can be simplified:

$$\mathbf{f}^{(e)} = \begin{Bmatrix} \mathbf{f}_1^{(e)} \\ \mathbf{f}_2^{(e)} \end{Bmatrix}, \ \mathbf{f}_i^{(e)} = \frac{l^{(e)}}{2} \begin{Bmatrix} f_z \\ m \end{Bmatrix} \int_{-1}^{1} N_i d\xi = \frac{l^{(e)}}{2} \begin{Bmatrix} f_z \\ m \end{Bmatrix} \tag{2.36}$$

$$\mathbf{f}_1 = \mathbf{f}_2 == \frac{l^{(e)}}{2} \begin{Bmatrix} f_z \\ m \end{Bmatrix} \tag{2.37}$$

i.e. the total distributed vertical forces and moments are split equally between the two nodes[17]. Note that in contrast to the Euler-Bernoulli theory, the distributed forces are independent of the distributed moments. This is due to the independent interpolation of the rotation and deflection, and as a consequence of this, the demand of continuity for the interpolation is only C^0. The integration is undertaking using the *Gaussian quadrature rule*:

$$\mathbf{K}^{(e)} = \sum_{p=1}^{n_p} \mathbf{B}_b^T EI_y \mathbf{B}_b W_p \frac{l^{(e)}}{2} + \sum_{p=1}^{n_p} \mathbf{B}_s^T GA^* \mathbf{B}_s W_p \frac{l^{(e)}}{2} \tag{2.38}$$

As mentioned earlier, splitting the element stiffness matrix into a bending and shear part can be more convenient. This makes it easier to identify the contributions from the different forces and makes it easier to apply a different order of integration to the different contributions. The latter can be useful when trying to abolish the defect from shear locking. This will be elaborated in the following section.

2.2 Shear locking

In order to illustrate the effect of shear locking, a cantilever beam with a concentrated load applied at the free end is modelled with both the Euler-Bernoulli and the Timoshenko theory. For simplicity, the beam is approximated with only one element. In this example the element stiffness matrix will be assembled separately for bending and shear. First the bending stiffness is assembled:

$$\mathbf{K}_b^{(e)} = EI_y \frac{l^{(e)}}{2} \int_{-1}^{1} \mathbf{B}_b^T \mathbf{B}_b d\xi \tag{2.39}$$

$$\mathbf{K}_b^{(e)} = EI_y \frac{l^{(e)}}{2} \int_{-1}^{1} \begin{bmatrix} 0 & -\frac{1}{l^{(e)}} & 0 & \frac{1}{l^{(e)}} \end{bmatrix}^T \begin{bmatrix} 0 & -\frac{1}{l^{(e)}} & 0 & \frac{1}{l^{(e)}} \end{bmatrix} d\xi \tag{2.40}$$

As the beam consists of one element $l^{(e)} = L$, and the matrix only contain constants, $\mathbf{K}_b$ can be integrated using only one Gauss point, yielding[]:

$$\mathbf{K}_b = \frac{EI_y}{2L}\begin{bmatrix} 0 & 0 & 0 & 0 \\ 0 & 1 & 0 & -1 \\ 0 & 0 & 0 & 0 \\ 0 & -1 & 0 & 1 \end{bmatrix} \tag{2.41}$$

Moving on to the $\mathbf{K}_s$:

$$\mathbf{K}_s = GA^* \frac{L}{2} \int_{-1}^{1} \left[-\frac{1}{l^{(e)}} \quad \frac{-(1-\xi)}{2} \quad \frac{1}{l^{(e)}} \quad \frac{-(1+\xi)}{2} \right]^T \left[-\frac{1}{l^{(e)}} \quad \frac{-(1-\xi)}{2} \quad \frac{1}{l^{(e)}} \quad \frac{-(1+\xi)}{2} \right] d\xi \tag{2.42}$$

$\mathbf{K}_s$ consists of quadratic terms of ξ, and in order to achieve exact integration two Gauss quadrature points have to be used, yielding:

$$\mathbf{K}_s = \frac{GA^*}{L}\begin{bmatrix} \frac{1}{L} & \frac{1}{2} & -\frac{1}{L} & \frac{1}{2} \\ \frac{1}{2} & \frac{L}{3} & -\frac{1}{2} & \frac{L}{6} \\ -\frac{1}{L} & -\frac{1}{2} & \frac{1}{L} & -\frac{1}{2} \\ \frac{1}{2} & \frac{L}{6} & -\frac{1}{2} & \frac{L}{3} \end{bmatrix} \tag{2.43}$$

Combining the two matrices and eliminating the clamped degrees of freedom yields:

$$\mathbf{K}_b = \begin{bmatrix} 0 & 0 \\ 0 & \frac{EI_y}{L} \end{bmatrix} \tag{2.44}$$

$$\mathbf{K}_s = \begin{bmatrix} \frac{GA^*}{L} & -\frac{GA^*}{2} \\ -\frac{GA^*}{2} & \frac{GA^*}{3}L \end{bmatrix} \tag{2.45}$$

$$\mathbf{K}_b + \mathbf{K}_s = \begin{bmatrix} \frac{GA^*}{L} & -\frac{GA^*}{2} \\ -\frac{GA^*}{2} & \left(\frac{GA^*}{3}L + \frac{EI_y}{L}\right) \end{bmatrix} \tag{2.46}$$

This combined matrix can be compared with the matrix deduced with the Euler-Bernoulli theory[18]:

$$\mathbf{K}_{EB} = \begin{bmatrix} \frac{12EI_y}{L^3} & -\frac{6EI_y}{L^2} \\ -\frac{6EI_y}{L^2} & \frac{4EI_y}{L} \end{bmatrix} \tag{2.47}$$

The Timoshenko element is expected to give the same results as the Euler-Bernoulli element for slender beams. To investigate this, the cantilever problem is solved using both elements with $P = 1$, starting with the Euler-Bernoulli element:

$$\begin{bmatrix} \frac{12EI_y}{L^3} & -\frac{6EI_y}{L^2} \\ -\frac{6EI_y}{L^2} & \frac{4EI_y}{L} \end{bmatrix} \begin{Bmatrix} w_2 \\ \theta_2 \end{Bmatrix} = \begin{Bmatrix} 1 \\ 0 \end{Bmatrix} \tag{2.48}$$

$$\begin{Bmatrix} w_2 \\ \theta_2 \end{Bmatrix} = \begin{bmatrix} \frac{L^3}{3EI_y} & \frac{L^2}{2EI_y} \\ \frac{L^2}{2EI_y} & \frac{L}{EI_y} \end{bmatrix} \begin{Bmatrix} 1 \\ 0 \end{Bmatrix} \tag{2.49}$$

$$w_2^{EB} = \frac{L^3}{3EI_y}, \quad \theta_2^{EB} = \frac{L^2}{2EI_y} \tag{2.50}$$

$$\begin{bmatrix} \frac{GA^*}{L} & -\frac{GA^*}{2} \\ -\frac{GA^*}{2} & \left(\frac{GA^*}{3}L + \frac{EI_y}{L}\right) \end{bmatrix} \begin{Bmatrix} w_2 \\ \theta_2 \end{Bmatrix} = \begin{Bmatrix} 1 \\ 0 \end{Bmatrix} \tag{2.51}$$

$$\beta = \frac{12EI_y}{L^2GA^*} = \frac{E}{Gk_z\lambda^2} \tag{2.52}$$

$$\begin{Bmatrix} w_2 \\ \theta_2 \end{Bmatrix} = \frac{\beta}{\beta+1} \begin{bmatrix} \left(\frac{L}{GA^*} + \frac{L^3}{3EI_y}\right) & \frac{L^2}{2EI_y} \\ \frac{L^2}{2EI_y} & \frac{L}{EI_y} \end{bmatrix} \begin{Bmatrix} 1 \\ 0 \end{Bmatrix} [17] \tag{2.53}$$

$$w_2^T = \frac{\beta}{\beta+1}\left(\frac{L}{GA^*} + \frac{L^3}{3EI_y}\right), \quad \theta_2^T = \frac{\beta}{\beta+1}\frac{L^2}{2EI_y} \tag{2.54}$$

As the slenderness of the beam increases, the solution from the Timoshenko element should approach the one obtained from the Euler-Bernoulli element:

$$r_w = \frac{w_2^T}{\frac{EB}{2}} = \frac{\beta}{\beta+1}\left(\frac{\frac{L}{GA^*} + \frac{L^3}{EI_y}}{\frac{L^3}{3EI_y}}\right) = \frac{3(4\lambda^2+3)}{4\lambda^2(\lambda^2+3)} \tag{2.55}$$

$$\lim_{\lambda\to\infty} \frac{3(4\lambda^2+3)}{4\lambda^2(\lambda^2+3)} = 0 \tag{2.56}$$

[17]

Equation 2.56 shows that instead of converging towards the Euler-Bernoulli solution, the solution from the Timoshenko element becomes progressively stiffer as the slenderness increases. This is due to the phenomena of *shear locking*. Numerous methods have been developed to eliminate this defect from the Timoshenko beam element. In this paper the method of *reduced integration* and *residual bending flexibility (RBF)* is elaborated in the following sections.

2.3 Reduced integration

Reduced integration is a popular and effective countermeasure to shear locking. To understand how and why this works, let us first take a look at Hughes's heuristic approach, the *constraint count method*[6]. Hughes's method revolves around comparing the *constraint ratio* from the continuous problem with the discretized one introduced by the FE formulation. The constraint ratio of the continuous problem is defined by the number of equilibrium equations divided by the number of the constraint equations, this is illustrated in equation 2.57 for 1D problems:

$$r_{cont} = \frac{n_{eq}}{n_c} = \frac{2}{1} \tag{2.57}$$

The discretized constraint ratio is defined by the limit case where the number of elements approaches infinity:

$$r_{disc} = \lim_{n_e \to \infty} \frac{n^e_{dofs}}{n_g} \tag{2.58}$$

Here n^e_{dofs} is the number of unknowns added by adding an additional element, whilst n_g is the number of Gauss points used. For optimal representation of the continuous problem, the two constraint ratios should be equal. Failing to satisfy this criteria indicates that the element is prone to locking. Adding an additional element gives one additional node, and with it two additional unknowns, giving the constraint ratio:

$$r_{disc} = \frac{2}{n_g} \tag{2.59}$$

To satisfy Hughes criteria, only one Gauss points has to be used. Recalling the integration of the shear stiffness matrix in Section 2.3, two Gauss points were used. Revisiting the example, this time under-integrating the shear stiffness matrix, by using only one Gauss point in accordance to Hughes's criteria, yields the following solution:

$$\begin{Bmatrix} w_2 \\ \theta_2 \end{Bmatrix} = \begin{bmatrix} \left(\frac{L}{GA^*} + \frac{L^3}{4EI_y}\right) & \frac{L^2}{2EI_y} \\ \frac{L^2}{2EI_y} & \frac{L^2}{EI_y} \end{bmatrix} \begin{Bmatrix} 1 \\ 0 \end{Bmatrix} [17] \tag{2.60}$$

The solution is once again tested against the Euler-Bernoulli solution[17]:

$$r_w = \frac{w_2^T}{w_2^{EB}} = \frac{3\lambda^2 + 3}{4\lambda^2} \tag{2.61}$$

$$\lim_{\lambda \to \infty} \frac{3\lambda^2 + 3}{4\lambda^2} = \frac{3}{4} \tag{2.62}$$

Now the end displacement ratio converge to 0.75, which is a significant improvement, and can be further improved by refining. By using 4 elements, the ratio is up to 0.984, thus shear locking is eliminated for this particular problem.

2.4 Residual bending flexibility, RBF

To further enhance a 2-noded element, residual bending flexibility (RBF) can be introduced. Proposed by MacNeal[8], RBF utilizes a substitute shear modulus, $\overline{GA}^*$, to improve nodal solutions independent of the slenderness of the problem. $\overline{GA}^*$ is obtained by equalling F_{11} of the flexibility matrices deduced with and without reduced integration, and replacing GA^* in the

expression from the reduced integration with $\overline{GA}^*$[17]:

$$\frac{L}{\overline{GA}^*} + \frac{L^3}{4EI_y} = \frac{L}{GA^*} + \frac{L^3}{3EI_y} \tag{2.63}$$

$$\frac{1}{\overline{GA}^*} = \frac{1}{GA^*} + \frac{L^2}{12EI_y} \tag{2.64}$$

$\overline{GA}^*$ then replaces GA^* in the stiffness matrix deduced from reduced integration. To avoid complicated expressions, K_1, K_2 and β from Section 2.3 is introduced:

$$K_1 = \frac{EI_y}{L^3}, \quad K_2 = 1 + \beta \tag{2.65}$$

The influence of the transverse shear strain is now only included in K_2. Expressing the enhanced matrix in K_1 and K_2 yields[17]:

$$\mathbf{K} = \begin{bmatrix} 12\frac{K_1}{K_2} & 6L\frac{K_1}{K_2} & -12\frac{K_1}{K_2} & 6L\frac{K_1}{K_2} \\ 6L\frac{K_1}{K_2} & K_1 + \frac{3K_1}{K_2} & -6L\frac{K_1}{K_2} & \frac{3K_1}{K_2} - K_1 \\ -12\frac{K_1}{K_2} & -6L\frac{K_1}{K_2} & 12\frac{K_1}{K_2} & -6L\frac{K_1}{K_2} \\ 6L\frac{K_1}{K_2} & \frac{3K_1}{K_2} - K_1 & -6L\frac{K_1}{K_2} & K_1 + \frac{3K_1}{K_2} \end{bmatrix} \tag{2.66}$$

As the slenderness approaches zero, $\beta \to 0$ and $K_2 \to 1$, the contribution from shear disappears, thus eliminating the effects from shear locking[17].

Chapter 3

Nonlinear Equilibrium Equations

In *Finite Element Analysis* (FEA), the response of the structure is expected to be linear. However, for many problems this is not the case. For structural problems, the nonlinearities can come from several sources, such as geometric nonlinearity, material nonlinearity, load nonlinearity and boundary condition nonlinearity. The physical source of geometric nonlinearity emerges when the change in geometry from the structure deforming, affects the kinematic and equilibrium equations. This can occur for slender structures, stability problems or tensile structures, such as cables or inflatable membranes[12]. This leads to a nonlinear *strain-displacement operator*, $[\partial]$, now being dependent on the displacements, u[12]:

$$\{\varepsilon\} = [\partial]\{u\} \tag{3.1}$$

This in turns effect the relation between strains and stresses, as the transposed strain-displacement operator is no longer guaranteed to be equal to the operator applied to the stresses.

$$[\bar{\partial}]^T \neq [\partial]^T \tag{3.2}$$

In FEA the materials is assumed to follow Hooke's generalized law.

$$\{\sigma\} = [E]\{\varepsilon\} \tag{3.3}$$

However, this is often not the case, as there are a variety of different phenomena that causes the material to behave in a nonlinear fashion. Take for instance work hardening or yielding of a metal or even creep. For all these phenomena, the material behaviour depends on either the current deformation state, or the history of deformation. As a consequence, the relation of strains and stresses in Hooke's law is no longer linear:

$$\{\sigma\} = [E](\{\varepsilon\} - \{\varepsilon_0\}) \tag{3.4}$$

For the load nonlinearities, the load becomes dependent on the displacements. This can typically occur for structures subjected to e.g. fluid loads, or other geometry sensitive types of loading. Both the prescribed surface tractions and body forces may now be dependent on the displacements of the structure:

$$\{F\} = \{F(u)\} \quad and \quad \{\Phi_c\} = \{\Phi_c(u)\} \tag{3.5}$$

The most important source of displacement boundary nonlinearities is the contact problem. In this case, the prescribed displacements would depend on the unknown displacements, as the contact would introduce new resistance

to the structure. The prescribed displacements now become a function of the unknown ones:

$$\{u_c\} = \{u_c(u)\} \tag{3.6}$$

Common for all of these cases, is that the linear relation between loads and displacements can no longer be used, so the nonlinear relation is introduced, were both the stiffness and the load becomes functions of the displacements:

$$[K(u)]\{u\} = \{R(u)\} \tag{3.7}$$

3.1 Solving Nonlinear Equilibrium Equations

To solve the nonlinear *force-displacement* relation presented in the previous section, an iterative approach is developed. The first step is to "guess" a displacement, called the *predictor step*. To evaluate how good the initial guess, u_1, has been, *the residual force*, R_{res}, is introduced. The residual force represents the out of balance forces, by comparing the external and internal forces in the structure.

$$\{R_{ext}\} - \{R_{int}\} = \{R_{res}\} \tag{3.8}$$

By doing a Taylor series expansion of the residual force at the state of u_1, and neglecting the higher order terms, yields the incremental equilibrium equation[12]:

$$R(u) \cong R_1 + \left(\frac{dR_1}{du}\right)(u - u_1) = 0 \tag{3.9}$$

The gradient of the incremental equilibrium equation is called the *tangent stiffness matrix*, K_T, and by taking the inverse of K_T, yields an expression for Δu, and further a new approximation for the displacement:

$$\Delta u_1 = -\left(\frac{dR_1}{du}\right)^{-1} R_1, \quad u_2 = u_1 + \Delta u_1 \tag{3.10}$$

Then a new and hopefully smaller residual force is calculated, using the new approximation. This procedure is repeated until the residual force reaches a prescribed tolerance[14]:

$$R_{res} \leq R_{tol} \tag{3.11}$$

This is called a Newton-Raphson iteration. Combining this with a forward Euler load incrementation, is one of the most common and simplest methods to solve the nonlinear equations. For the *full Newton-Raphson*, the load is applied in increments and the convergence for each increment is obtained before proceeding to the next. This is illustrated in with an algorithm in Figure 3.1[14]:

If the tangent stiffness, K_T, is calculated for every step, the method is classified as a *full* or *true Newton-Rahpson*. Although this is a reliable method for many problems, the majority of computational time is spent updating the K_T. To reduce the computational effort, several methods have been proposed, modifying the full Newton-Raphson, but they will not be elaborated in this paper.

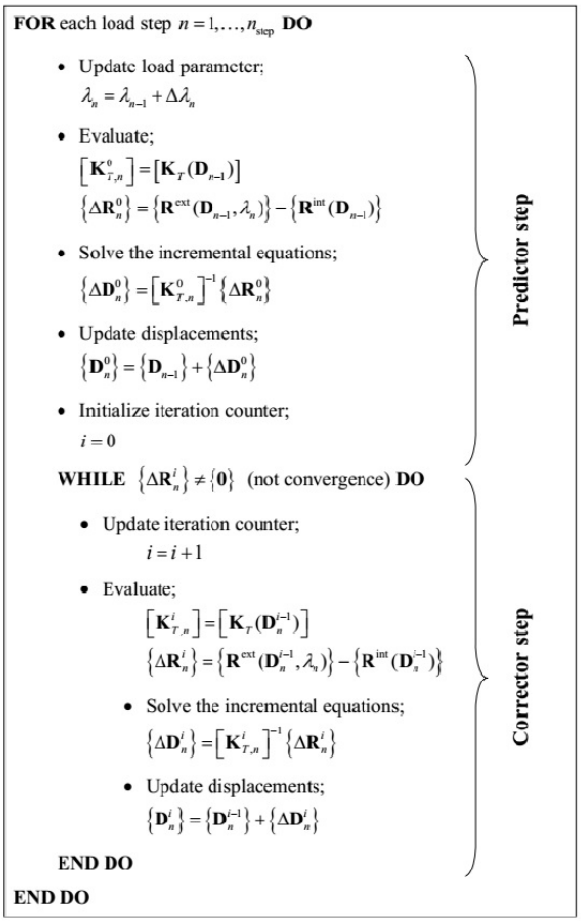

Figure 3.1: Algorithm describing the full Newton-Rahpson, note that **u** has been replaced by **D** in the figure

3.2 Nonlinear Dynamic Equilibrium Equations

In dynamics a linear problem can for the most be studied by using modal methods in the frequency domain. This is not the case for nonlinear problems. For a nonlinear problem the equations of motion requires direct integration, and there are two different methods available, the *explicit scheme* and the *implicit scheme*. As always, both methods have advantages and disadvantages. Throughout this section the two methods will be explained and their advantages and disadvantages compared, starting with the explicit scheme.

The explicit scheme obtains the solution through known quantities, the dynamic equilibrium at the time t_n is used to calculate the displacements of t_{n+1}. For a diagonal lumped mass matrix, the accelerations at the beginning of a given increment can be obtained through Equation 3.12[13]:

$$\{\ddot{\mathbf{D}}\} = [\mathbf{M}]^{-1}(\{\mathbf{R}^{ext}\}_{n+1} - \{\mathbf{R}^{damp}_{n+1/2}\} - \{\mathbf{R}^{int}\}_{n+1}) \tag{3.12}$$

A major advantage of the explicit method, is that neither a tangent stiffness matrix, a iteration check nor a convergence check is needed, making each time increment quite cheap in computational effort. Most of the computational effort is associated with calculating the element forces and assembling the force vectors. It is possible to reduce computational effort further by minimizing the number of Gauss points used in integration, thus making reduced integration discussed in Section 2.3, a very attractive method for explicit schemes. However, the explicit scheme has one big disadvantage, the scheme is only *conditionally stable*[13]. For unstable linear problems the instability blows up and grows infinitely, and is thus easy to detect. The

nonlinear instability on the other hand, can be much harder to detect, as the artificially introduced energy can be dissipated by e.g. elastic-plastic material behaviour, making it an even worse attribute[13]. For the explicit scheme the time step, Δt has to be less than the *stable time increment* Δt_{cr}. Δt_{cr} can be found by looking at the eigenfrequencies, ω_j, and the *fraction of critical damping*, ξ_j. Assuming that the damping is small for all modes, Δt_{cr} can be found for the highest natural frequency[13]:

$$\Delta t_{cr} \leq \frac{2}{\omega_{max}}(\sqrt{1-\xi^2} - \xi) \tag{3.13}$$

For a system without damping, Δt_{cr} can be found by:

$$\Delta t_{cr} \leq \frac{2}{\omega_{max}} \tag{3.14}$$

Δt_{cr} can also be expressed in the minimum time it takes a dilatational wave to travel across the smallest element in the model[13]:

$$\Delta t_{cr} = \frac{l^{(e)}}{c_d}, \quad with \quad c_d = \sqrt{\frac{E}{\rho}} \tag{3.15}$$

Note that the material properties that effect Δt_{cr}, are the instantaneous values.

Summing up the explicit scheme, it is a simple method with low computational cost for each time step, but it needs a very small time step in order to remain stable. To check whether the scheme is stable, an energy balance for the model can be evaluated.

In contrast to the explicit scheme, the implicit scheme requires solving of the nonlinear algebraic equations for every time step. The scheme also needs

to obtain convergence for each increment, and this is usually done with a Newton-Rahpson iteration, discussed in Section 3.1. By assuming that the internal forces are functions of displacements only, the approximation for $\{R^{int}\}_{n+1}$ can be written as[13]:

$$\{\mathbf{R}^{int}\}_{n+1} = \{\mathbf{R}^{int}\}_n + \left[\frac{\partial \mathbf{R}^{int}}{\partial \mathbf{D}}\right]_n \{\Delta \mathbf{D}\} \quad with \quad \left[\frac{\partial \mathbf{R}^{int}}{\partial \mathbf{D}}\right]_n = [\mathbf{K}_T]_n \tag{3.16}$$

With this in place, the equation of motion at t_{n+1} can be written as:

$$[\mathbf{M}]\{\ddot{\mathbf{D}}\}_{n+1} + [\mathbf{C}]\{\dot{\mathbf{D}}\}_{n+1} + [\mathbf{K}]_T\{\mathbf{D}\} = \{\mathbf{R}^{ext}\}_{n+1} - \{\mathbf{R}^{int}\}_n \tag{3.17}$$

By applying Newmark approximations the velocities and accelerations can be estimated by:

$$\{\ddot{\mathbf{D}}\}_{n+1} = \frac{1}{\beta \Delta t^2}(\{\mathbf{D}\}_{n+1} - \{\mathbf{D}\}_n - \Delta t\{\dot{\mathbf{D}}_n) - \left(\frac{1}{2\beta} - 1\right)\{\ddot{\mathbf{D}}_n \tag{3.18}$$

$$\{\dot{\mathbf{D}}\}_{n+1} = \frac{\gamma}{\beta \Delta t}(\{\mathbf{D}\}_{n+1} - \{\mathbf{D}\}_n) - \left(\frac{\gamma}{\beta} - 1\right)\{\dot{\mathbf{D}}_n - \Delta\} t \left(\frac{\gamma}{2\beta} - 1\right)\{\ddot{\mathbf{D}}_n\} \tag{3.19}$$

The *effective stiffness matrix*, $\mathbf{K}^{eff}$, and the *effective residual force vector*,

$\mathbf{R}^{eff}$ are defined as:

$$[\mathbf{K}^{eff}]_n = \frac{1}{\beta\Delta t^2}[\mathbf{M}] + \frac{\gamma}{\beta\Delta t}[\mathbf{C}] + [\mathbf{K}_T]_n \tag{3.20}$$

$$\{\mathbf{R}^{eff}\}_{n+1} = \{\mathbf{R}^{ext}\}_{n+1} - \{\mathbf{R}^{int}\}_n + [\mathbf{M}]\left[\frac{1}{\beta\Delta t}\{\dot{\mathbf{D}}\}_n + \left(\frac{1}{2\beta} - 1\right)\{\ddot{\mathbf{D}}\}_n\right] + [\mathbf{C}]\left[\left(\frac{\gamma}{\beta} - 1\right)\{\dot{\mathbf{D}}\}_n + \Delta t\left(\frac{\gamma}{2\beta} - a\right)\{\ddot{\mathbf{D}}_n\right]$$

The two combined yields the equation of motion on incremental form[13]:

$$[\mathbf{K}^{eff}]_n\{\Delta\mathbf{D}\} = \{\Delta\mathbf{R}^{eff}\}_{n+1} \tag{3.21}$$

Introducing numerical damping to the Newmark method degrades the order of accuracy, and it is therefore recommended to use the *HHT α-method* to retain second order of accuracy. As opposed to linear problems, the implicit scheme is not unconditionally stable for nonlinear problems. In order to avoid instability, Newton-Raphson should be performed to enforce equilibrium. In order for a HHT α-method to be stable for linear problems, the following criterias have to be met[16]:

$$-\frac{1}{3} \leq \alpha_h \leq 0, \quad \gamma = \frac{1}{2}(1 - 2\alpha_h), \quad \beta = \frac{1}{4}(1 - \alpha_h)^2 \tag{3.22}$$

Summing up the implicit scheme, the time steps are computational expensive due to the need of solving the nonlinear equilibrium equations at each time step, as well as the need to obtain convergence for each increment. Although the implicit scheme is not guaranteed to be unconditionally stable

for nonlinear problems, it can run with a much bigger time step than the explicit scheme.

3.3 Strain measures for large deformations

To be able to compare the two FEA formulations applied in Chapter 4, it is important to look into the strain measures the formulations utilizes. The *Green-Lagrange strain measure* used by Abaqus, and the *Biot strain measure*, utilized by the geometrically exact element used in Chapter 4.

To represent large deformations, the displacement vector $\mathbf{u}$ is introduced. The displacement vector is defined by taking the position vector of the deformed configuration, $\mathbf{x}$, and subtracting the position vector from the reference configuration, $\mathbf{X}$[19].

$$\mathbf{u} = \mathbf{x} - \mathbf{X} \tag{3.23}$$

This is illustrated in Figure 3.2

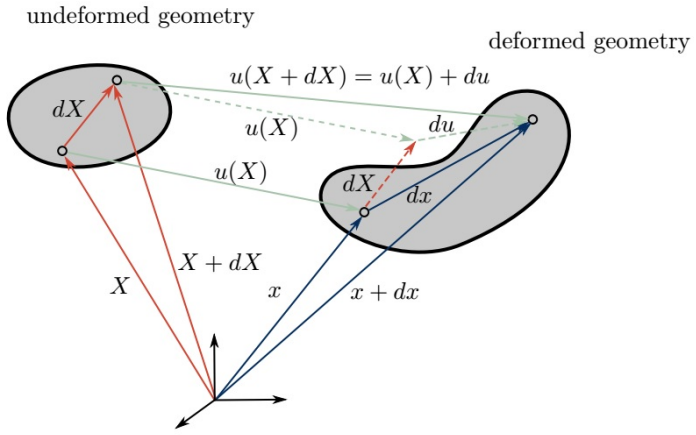

Figure 3.2: Geometry description for large deformations in a Cartesian coordinate system[19]

In order to apply a mapping between a differential line element in the reference configuration to the deformed configuration, the deformation gradient, $\mathbf{F}$, is introduced:

$$d\mathbf{x} = \mathbf{F}d\mathbf{X} \tag{3.24}$$

F is defined by the base vectors, and can be used to map between them[19]:

$$\mathbf{F} = g_i \otimes G^i, \quad \mathbf{F}^T = G^i \otimes g_i, \quad \mathbf{F}^{-1} = G_i \otimes g^i, \quad \mathbf{F}^{-T} = g^i \otimes G_i \tag{3.25}$$

Further the **F** is used to find the *Green-Lagrange strain tensor*, **E**.

$$\mathbf{E} = \frac{1}{2}(\mathbf{F}^T\mathbf{F} - \mathbf{I}) \tag{3.26}$$

I is the *identity tensor*, and by using the relations from Equation 3.25, the Green-Lagrange tensor can be rewritten:

$$\mathbf{E} = \frac{1}{2}((\mathbf{G}^i \otimes \mathbf{g}_i)(\mathbf{g}_j \otimes \mathbf{G}^j) - G_{ij}\mathbf{G}^i \otimes \mathbf{G}^j) = \frac{1}{2}(g_{ij} - G_{ij})\mathbf{G}^i \otimes \mathbf{G}^j \tag{3.27}$$

$$\mathbf{E} = E_{ij}\mathbf{G}^i \otimes \mathbf{G}^j \tag{3.28}$$

E_{ij} is the *Green-Lagrange* coefficients and is obtained through the metric coefficients, g_{ij} and G_{ij}, who determines the length and angle between the base vectors[19]. The Green-Lagrange strain measure describes a nonlinear relation between the displacements and strains, and is well suited to measure strains under large deformations.

For the geometrically exact beam model the beam geometry is defined by a centroid line B with an attached cross-section A. The centroid of the reference configuration is defined by $\mathbf{X}(S)$ and the deformed configuration is defined by $\mathbf{x}(S,t)$, with S being the arc-length parameter. Both the reference and the deformed configuration, have a local Cartesian coordinate system, that travels along the centroid, denoted $\{\mathbf{i}_i^0\}_{i=1,2,3}$ for the reference configuration, and $\{\mathbf{i}_i\}_{i=1,2,3}$ for the deformed configuration. The local coordinate system travels along the centroid in such a way that the cross-section is always perpendicular to $\mathbf{i}_1$. This and the other geometric quantities is depicted in Figure 3.3[15].

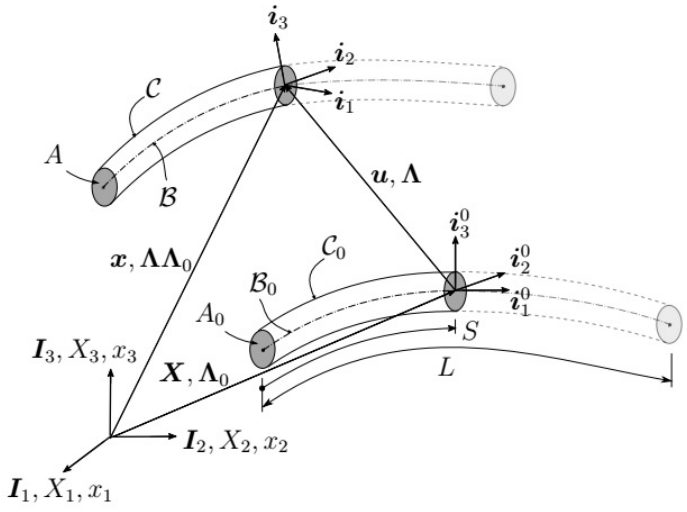

Figure 3.3: Geometry description for large deformations for the GE beam model[15]

To keep track of the orientation of the local coordinate system along S,

the two-point tensor $\Lambda(S,t)$ is defined, such that[15]:

$$\mathbf{i}_i(S,t) = \Lambda(S,t)\mathbf{i}_i^0(S) \Rightarrow \Lambda(S,t) = \mathbf{i}_i \otimes \mathbf{i}_i^0 \tag{3.29}$$

$$||\mathbf{i}_i|| = ||\mathbf{i}_i^0|| = 1 \tag{3.30}$$

$$\Lambda^T\Lambda = \mathbf{I} \tag{3.31}$$

Defining the reference and deformed configuration with respect to the Cartesian frame $\mathbf{I}_i$, the transformation gives:

$$\mathbf{i}_i(S,t) = \Lambda(S,t)\Lambda_0(S)\mathbf{I}_i \Rightarrow \Lambda_0(S) = \mathbf{i}_i^0 \otimes \mathbf{I}_i \tag{3.32}$$

The deformed configuration, C may now be uniquely determined, by the deformed position and the rotation of the centroid[15].

$$C = \{\varphi = (\mathbf{x}, \Lambda) : [0,L] \times [0,T] \to \mathbb{R}^3 \times SO(3)\} \tag{3.33}$$

$SO(3)$ represents the group of all rotations about the origin of $\mathbb{R}^3$ under the operation of composition. This means that the kinematics of the beam, is reduced to a 1D description, with only the arc length coordinate, S, as a parameter. The 3D beam geometry can now be defined by:

$$\mathbf{x}^{3D}(S, x_\alpha^0, t) = \mathbf{x}(S,t) + \mathbf{p}(S, x_\alpha^0, t) = \mathbf{x}(S,t) + \Lambda(S,t)x_\alpha^0 i_\alpha^0(S) \tag{3.34}$$

Where $p(S, x_\alpha^0)$ is the position vector of a point of the geometry, and α denotes the two directions parallel to the cross-section. With $\mathbf{x}^{3D}$ the deformation gradient, $\mathbf{F}$ can be found:

$$\mathbf{F} = \frac{\partial \mathbf{x}^{3D}}{\partial x_i^0} \otimes \mathbf{i}_1^0 = (\mathbf{x}' + \Lambda' x_\alpha^0 \mathbf{i}_\alpha^0) \otimes \mathbf{i}_1^0 + \mathbf{i}_\alpha \otimes \mathbf{i}_\alpha^0 \tag{3.35}$$

Due to the parameterization of the rotations[15], Λ' can be expressed by a skew symmetric-tensor, $\tilde{\kappa}$:

$$\Lambda' = \tilde{\kappa}\Lambda \Leftrightarrow \tilde{\kappa} = \Lambda'\Lambda^T \tag{3.36}$$

By inserting $\tilde{\kappa}$ and by adding and subtracting $\mathbf{i}_1 \otimes \mathbf{i}_i^0$, the $\mathbf{F}$ can be written with a polar material decomposition:

$$\mathbf{F} = \Lambda\{\mathbf{I} + [\Lambda^T(\mathbf{x}' - \mathbf{i}_1) + \Lambda^T \tilde{\kappa} x_\alpha^0 \mathbf{i}_\alpha^0] \otimes \mathbf{i}_1^0\} = \Lambda\mathbf{U} \tag{3.37}$$

With $\mathbf{U}$ being the right (current local) stretch tensor, that the Biot strain measure can be derived from. The Biot strains are objective corotated engineering strains that are independent of rigid body motions. The Biot strain measure can be written as:

$$\mathbf{B} = \Lambda^T\mathbf{F} - \mathbf{I} = \mathbf{U} - \mathbf{I} = \varepsilon \otimes \mathbf{i}_1 \tag{3.38}$$

$$\varepsilon = \Lambda^T(\gamma + \tilde{\kappa}p) \tag{3.39}$$

With ε representing a generalized convected strain measure.

For interested readers the theory of the geometrically exact beam element is further elaborated in *A Comparative Study of Beam Element Formulations for Nonlinear Analysis: Corotational vs Geometrically Exact Formulations*, Kjell M. Mathisen et al.[15]

Chapter 4

Numeric results

Throughout this chapter a number of different cantilever problems will be solved using IFEM, an in-house software developed at SINTEF ICT, where geometrically exact elements are implemented, and ABAQUS. Through these tests, it is possible to study the convergence and accuracy of the elements and compare them. All of the examples undertaken in this chapter are various forms of slender cantilever beams, clamped at one end and loaded at the other. The examples induce bending and displacements in more than one direction, and to compare the results, the *norm of displacement* for both the solution and its corresponding reference solution has been used. The reference solution is found for each element by solving the problem with a very fine grid.

$$u = \sqrt{u_x^2 + u_y^2 + u_z^2}, \;\; u_{ref} = \sqrt{u_{x,ref}^2 + u_{y,ref}^2 + u_{z,ref}^2} \tag{4.1}$$

For the beam examples in question, the solutions obtained from the different elements are indistinguishable even for coarse refinements, as illustrated in Figure 4.1, were the coarse refinement of 10 2-noded GEQ1 elements coincides with 100 GEQ3 elements.

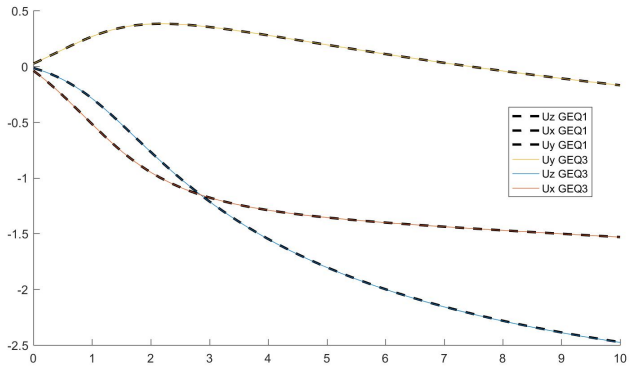

Figure 4.1: Displacement versus applied load for the Three legged beam, using a coarse refinement with GEQ1 and a fine refinement with GEQ3

In order to illustrate the difference in performance between the elements, *the relative error*, e_u, of the tip displacements and rotations have been plotted against the number of free nodes used by the element.

$$e_u = \frac{|u_{ref} - u|}{|u_{ref}|} \quad and \quad e_\theta = \frac{|\theta_{ref} - \theta|}{|\theta_{ref}|} \tag{4.2}$$

IFEM can run with an arbitrary polynomial order, but for these examples only elements of order 1, 2 and 3 have been used. All IFEM elements utilize reduced integration, discussed in Section 2.3, but the 2-noded element can

also be run with a RBF formulation, discussed in Section 2.4. IFEM will be compared with the shear flexible beam elements from ABAQUS, B31 and B32. One important difference between the ABAQUS and IFEM is the strain measure they utilize. IFEM utilizes the *Biot strain measure*, whilst ABAQUS utilizes the *Green-Lagrange strain measure*[10]. This means that ABAQUS needs to insert additional internal nodes to the prescribed ones in order to be able to run the simulations. These additional nodes have not been accounted for when the relative error has been plotted against the number of nodes. As long as the strains ranges from small to moderate, the two representations is expected to yield the same results, but ABAQUS may have an advantage over IFEM for coarse refinements.

4.1 Three legged beam

The three legged beam consists of three beams connected with 90 degree angles, in such a manner that each leg's beam axis is parallel to the x-, y- and z-axis. The relative error of displacement and rotation is plotted against the number of free nodes for each leg. The geometry and the beam properties are depicted in Figure 4.2.

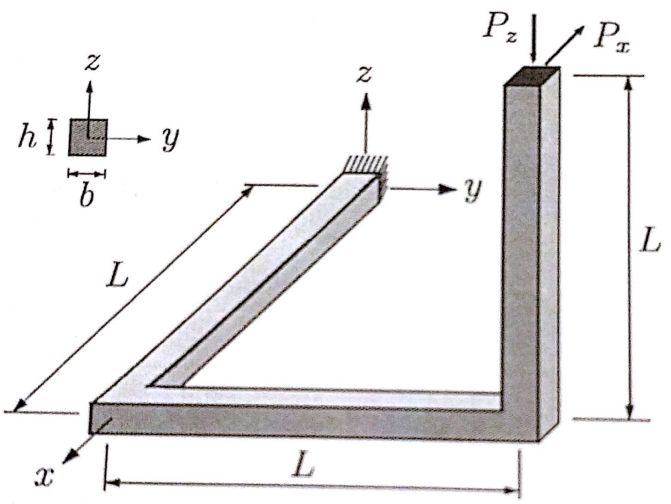

E	10^6
ν	0
L	1
b	0.1
h	0.1
P_x	10
P_z	10
λ	10

Figure 4.2: Geometry and loading of the three legged beam[15]

The beam is subjected to two concentrated loads, acting in the negative x- and z-directions. This loading induces shear stress, combined bending and torsion, and is well suited as a benchmark for testing nonlinear beam formulations.

Comparing the results from displacements of the 2-noded elements in Figure 4.3 on the left hand side, it seems as the GE RBF formulation slightly

outperforms the unenhanced formulation, and is almost coinciding with the solution from ABAQUS. However, looking at the rotations on the right hand side of Figure 4.3, the tables have turned and the unenhanced formulation now slightly outperforms the RBF formulation, whilst coinciding with the solution from ABAQUS.

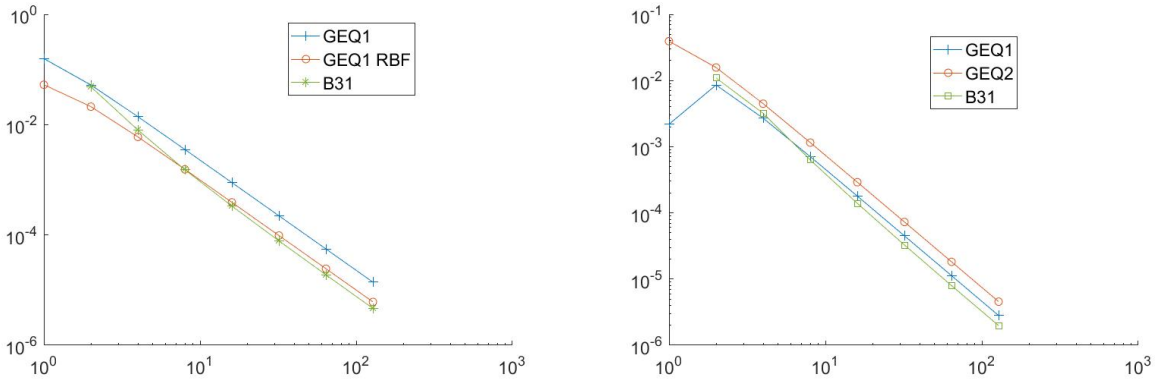

Figure 4.3: Displacement plot on the left and rotation plot on the right side for the 2-noded elements

Observing the results from the higher order elements plotted in Figure 4.4, the B32 element gives a better accuracy at the coarser meshes, but has a lower convergence rate than the quadratic GE element GEQ2. The increased accuracy at the coarser meshes can be due to the difference in strain measure between the elements, as mentioned earlier in this chapter. It is also worth noticing that the GEQ3's convergence rate has shifted approximately one order compared to the quadratic elements, as is to be expected judging from previous studies[15]. Figure 4.5 shows all the elements plotted together.

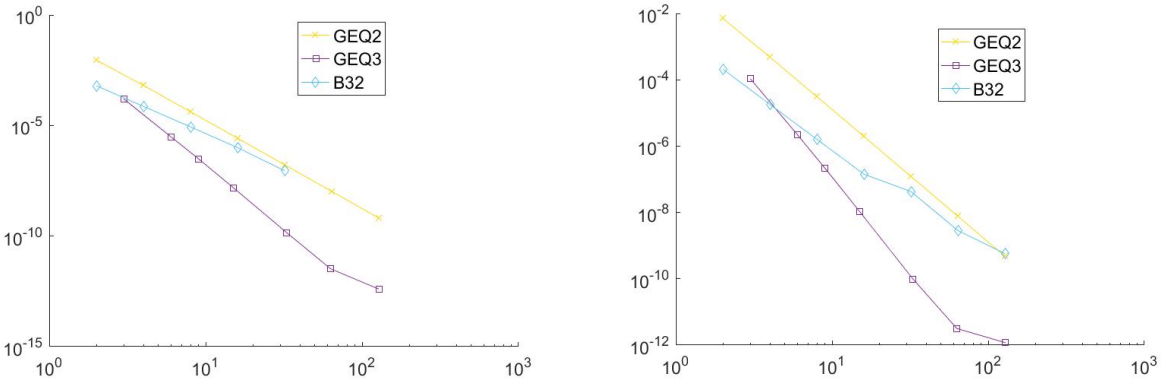

Figure 4.4: Displacement plot on the left and rotation plot on the right for the higher order elements

Looking at all the elements plotted together, it is clear to see that going from a 2-noded to a quadratic element, gives a significant increase in rate of convergence. While the difference in rate of convergence between the quadratic and cubic GE element is not as great, the initial accuracy is substantial, making the cubic element an attractive option.

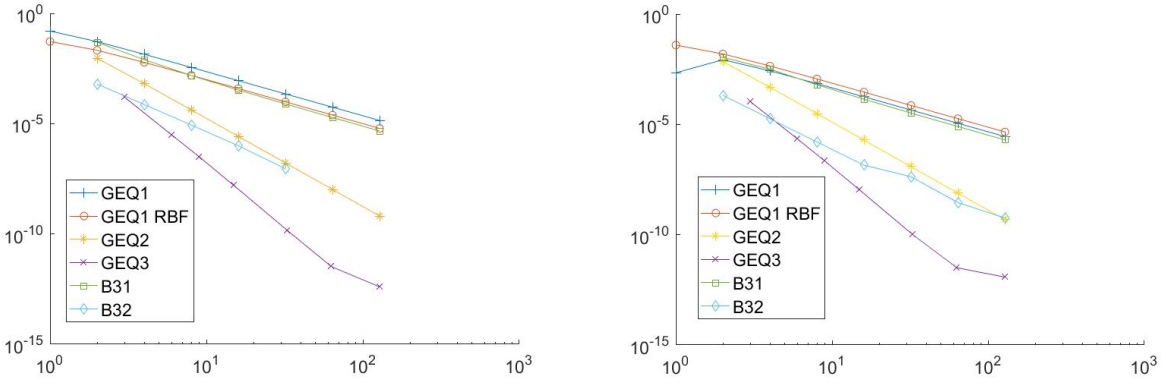

Figure 4.5: Displacement plot on the left and rotation plot on the right for all the elements

4.2 Curved beam

The second example is a curved beam oriented with its beam axis parallel to the xy-plane. The curved reference configuration is stress-free, and the beam's curvature follows that of a circle with a radius of 100. The beam is subjected to a concentrated load, acting at the free end in the positive z-direction. The geometry, loading and the beam properties are depicted in Figure 4.6.

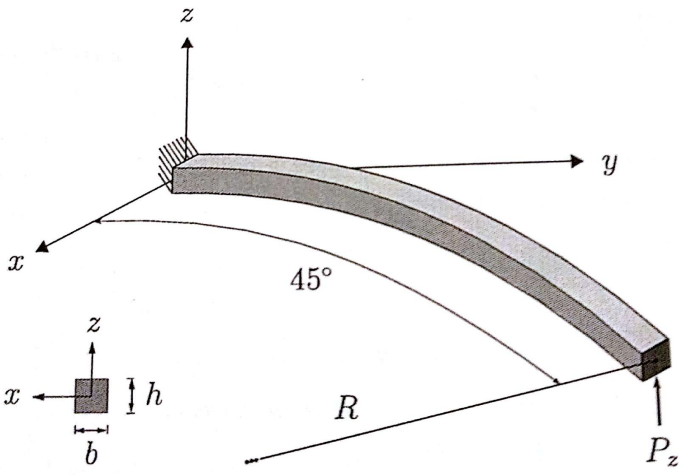

E	10^7
ν	0
L	1
b	1
h	1
P_x	10
P_z	10
λ	78

Figure 4.6: Geometry, loading and beam properties of the curved beam[15]

This is a popular benchmark problem, and has been presented by several authors[15][4][5][3][2]. Note that for this problem it was not possible to obtain an equally refined reference solution with the ABAQUS elements as with IFEM, with 500 elements for the B31 reference solution, 150 elements for the B32 reference solution, compared to the 1024 elements with IFEM. This can give the ABAQUS elements an edge in accuracy, so it is more interesting to have a look at the rate of convergence when comparing it with the GE

elements.

In the displacement plot on the left in Figure 4.7, the two RBF formulations outperforms the unenhanced formulation, and coincides for increased refinement. The difference between the two formulations at the coarser meshes can be due to ABAQUS's internal nodes, and due to the lesser refinement of the B31 reference solution. For the rotations on the right side, the unenhanced formulation fare a little better, but still falls behind the two RBF elements. The GE enhanced element comes a little short compared with the accuracy of the B31 element, but the rate of convergence for all the 2-noded elements are still equal.

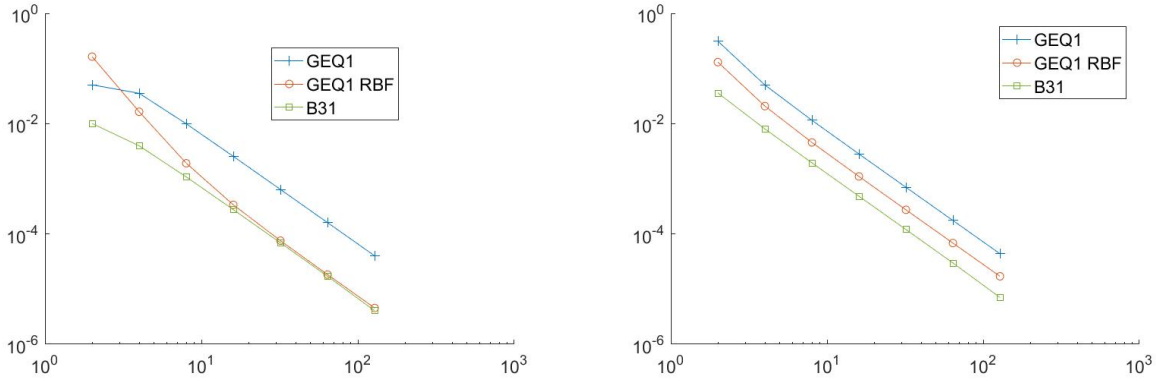

Figure 4.7: Displacement plot on the left and rotation plot on the right for the 2-noded elements

The quadratic elements plotted in Figure 4.8, seems to be performing equally, and coinciding for the majority of the refinements. The kink of the B32 line for the rotations, is most likely due to the poor reference solution. The accuracy of the cubic GE element is once again about one order higher compared to the quadratic ones, but for this problem, the rate of convergence

is equal.

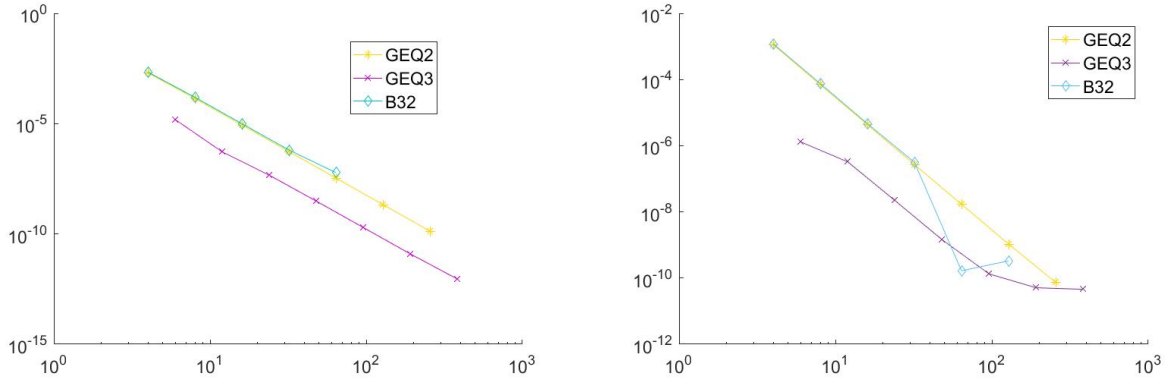

Figure 4.8: Displacement plot on the left and rotation on the right for the higher order elements

With all the elements plotted together in Figure 4.9, it is clear to see the advantage of going for a higher order element for this problem, both when it comes to displacements and rotations. As an example, to achieve the accuracy of displacement for two elements of the cubic GE element, the RBF elements need 74 elements. As an illustration, all the elements have been plotted again in Figure 4.10, but this time the ABAQUS elements are plotted against the actual number of nodes, both the prescribed and the added internal nodes. Figure 4.10 tells quite a different tale, compared to Figure 4.9. This time the unenchanced GE element coincides with B31, whilst the GE RBF element outperforms them both by approximately one order of accuracy. The same pattern is visible for the higher order elements, were the GE elements is outperforming the ABAQUS B32 significantly in accuracy. Note that this may not be a fair representation, as it is not documented how many new degrees of freedom one internal node adds to the system.

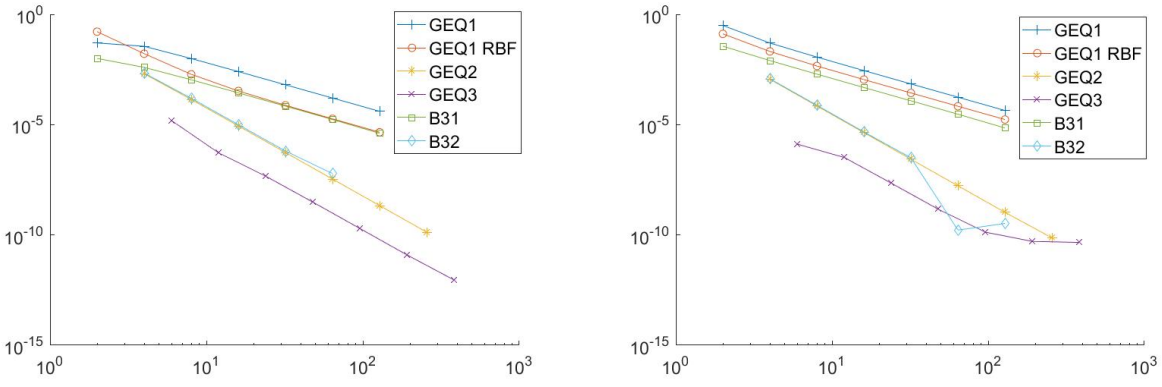

Figure 4.9: Displacement plot on the left and rotation plot on the right for all the elements

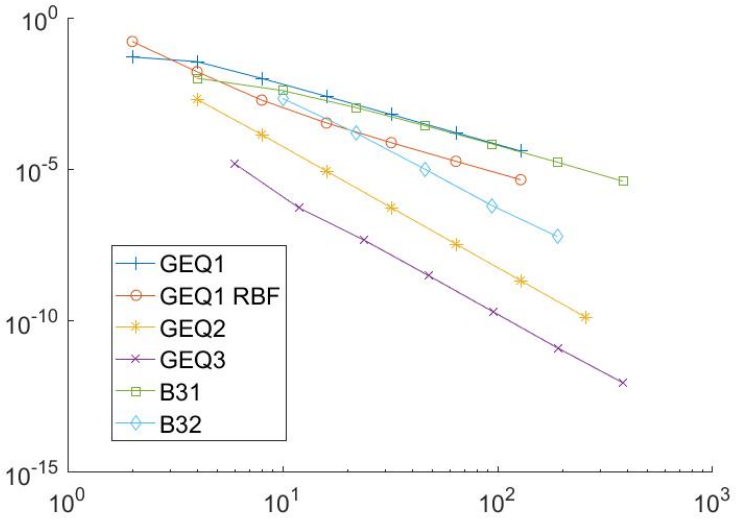

Figure 4.10: Displacement plot for all the elements, plotted against the actual number of nodes, including the internal nodes

4.3 Dynamic

The third example is a planar cantilever beam with symmetric cross-section, subjected to a dynamic sinusoidal load at the free end acting in the z-direction. The geometry, loading and the beam's properties are depicted in Figure 4.11. Similar examples have been undertaken by other authors[7].

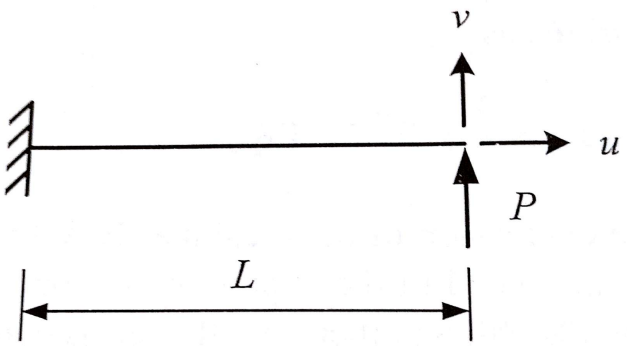

E	2.1×10^{11}
ν	0.3
ρ	7800
L	10
b	0.25
h	0.5
P_0	10^6
ω	50
P	$P_0 sin(\omega \times t)$
Δt	5.0×10^{-4}
α	-0.05
λ	50

Figure 4.11: Geometry, loading and beam properties for the cantilever subjected to dynamic loading[7]

For this nonlinear dynamic problem the time series of the displacement, the velocity and the acceleration are plotted, using the shear flexible beam elements, and the Euler-Bernoulli element B33 from ABAQUS. To get a fair comparison between the elements, the refinement of six free nodes have been used for all the formulations. Note that once again, the internal nodes produced in ABAQUS have not been taken into consideration when plotting. Table 4.1 gives the relation between the number of nodes and elements for the different formulations. The reference solution has been produced using GEQ3 with a refinement of 50 elements.

	GEQ1	GEQ1 RBF	GEQ2	GEQ3	B31	B33	B32
Elements	6	6	3	2	6	6	3
Nodes	7	7	7	7	7	7	7
Added nodes	0	0	0	0	12	6	9

Table 4.1: Number of nodes and elements needed for the different elements

In Figure 4.12 the two 2-noded elements from IFEM is compared. From the displacement plot, it seems like the RBF formulation is better at the beginning, but deteriorating towards the end of the series. Since there is no clear winner, the results from velocity and acceleration plots in Figure 4.13 and 4.14 must be studied. Once again, the RBF element outperforms the unenhanced formulation at the beginning of both series, before deteriorating towards the end, making it hard to pick a winner among the two elements.

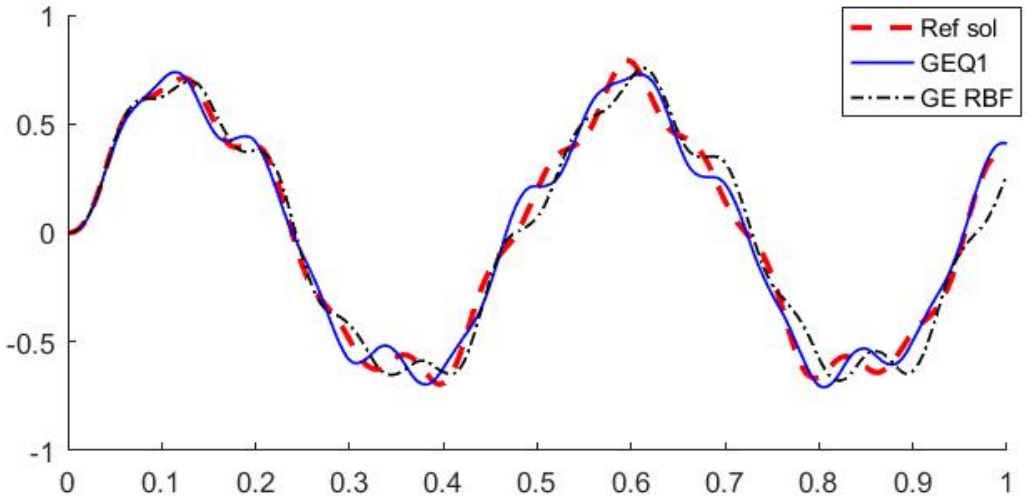

Figure 4.12: Displacement plot for the 2-noded GE elements

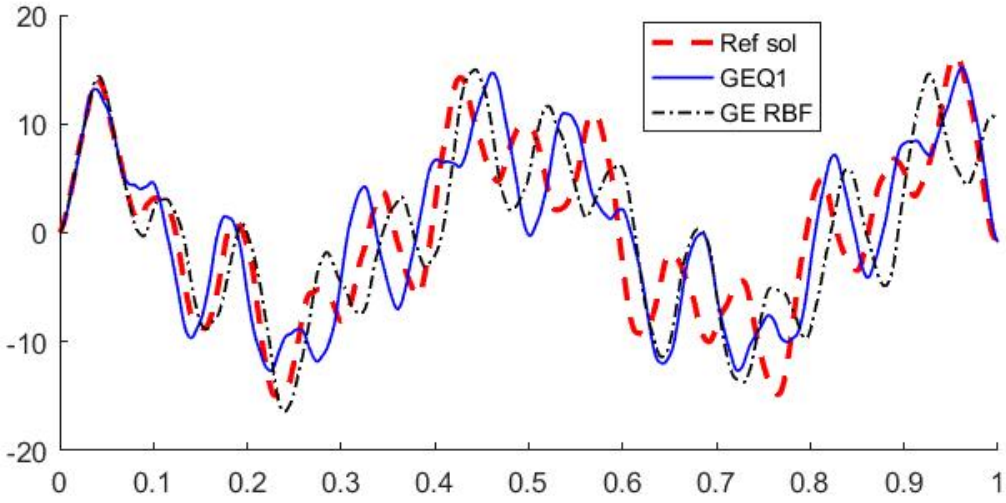

Figure 4.13: Velocity plot for the 2-noded GE elements

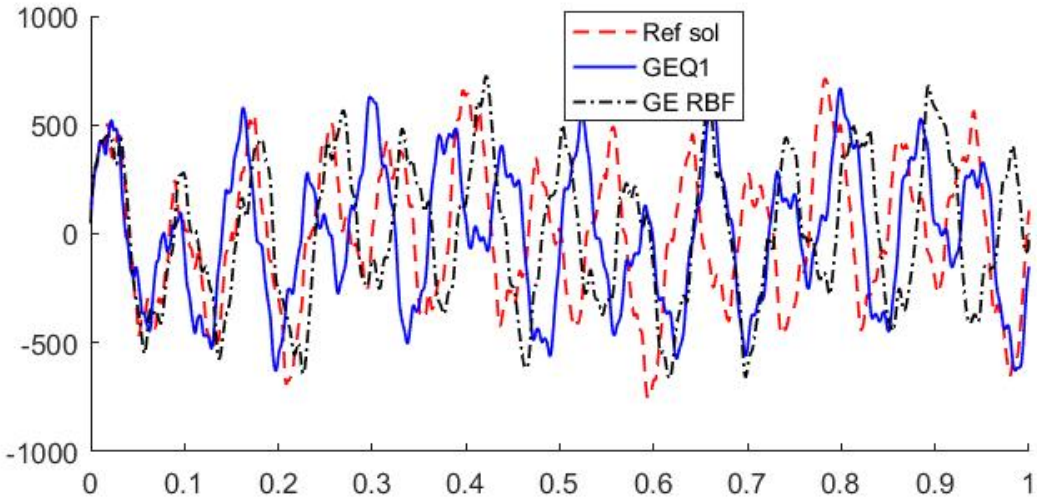

Figure 4.14: Acceleration plot for the 2-noded GE elements

In Figure 4.15, 4.16 and 4.17, the ABAQUS element slightly outperforms the GE element in the velocity and acceleration plots. This is most likely due to the internal nodes that gives ABAQUS an edge for coarse refinements.

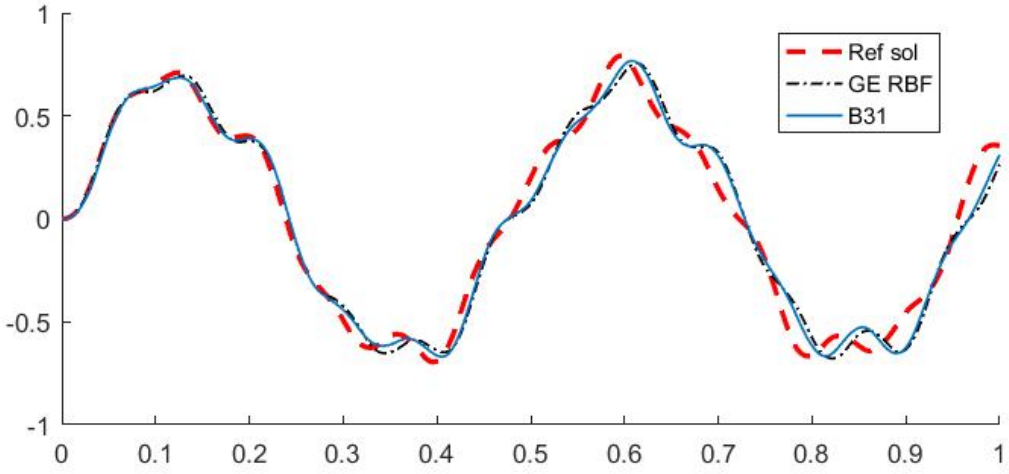

Figure 4.15: Displacement plot for the RBF enhanced elements

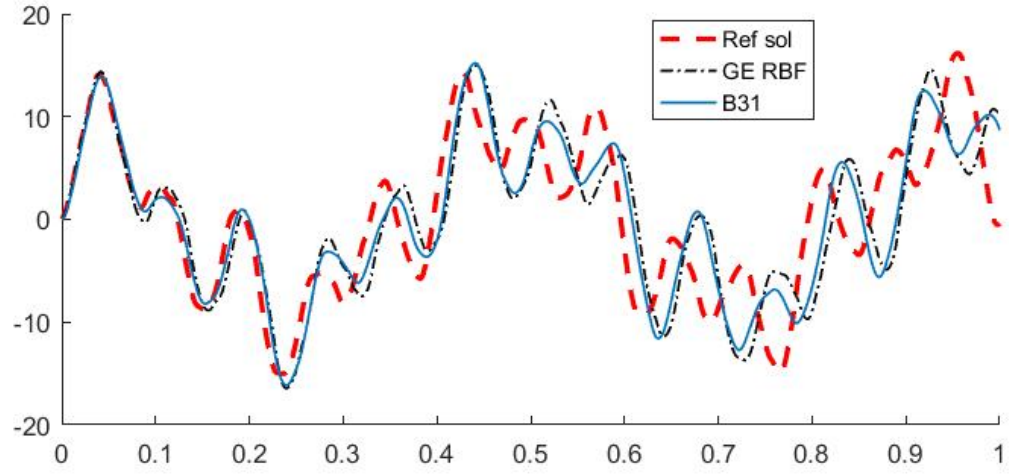

Figure 4.16: Velocity plot for the RBF enhanced elements

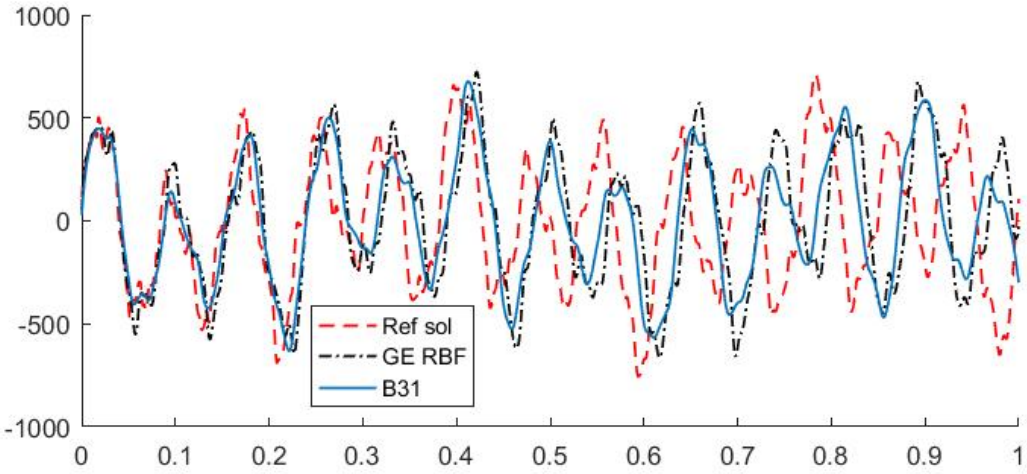

Figure 4.17: Acceleration plot for the RBF enhanced elements

In Figure 4.18, 4.19 and 4.20, the best 2-noded shear flexible element is tested against the Euler-Bernoulli element, B33. It is clear, already from the displacement plot in Figure 4.18, that the B33 element outperforms the B31 element. This is probably due to the representation of the mass matrix. The 2-noded shear flexible elements utilize the lumped mass matrix[11], whilst the Euler-Bernoulli element uses quadratic interpolation functions, and can use a consistent mass formulation, which is superior when it comes to distributed forces, like the ones from the d'Alembert inertia forces in a dynamic problem[9].

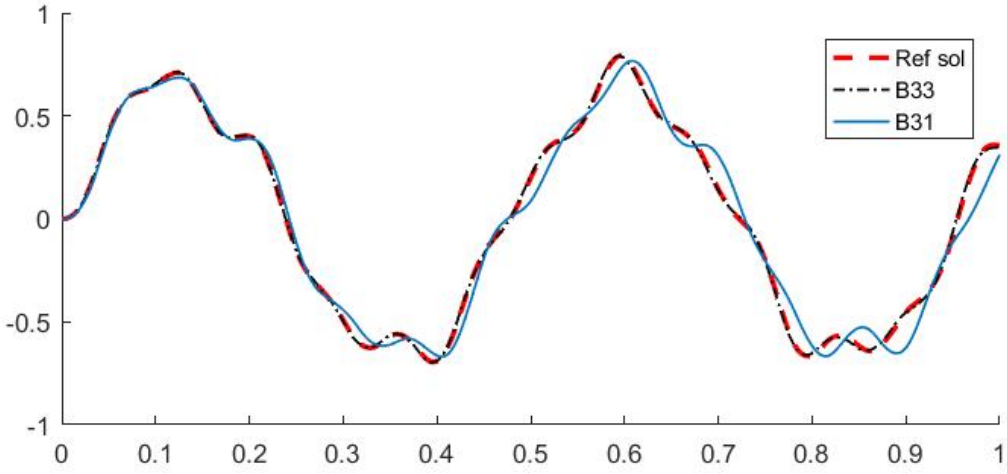

Figure 4.18: Displacement plot for the ABAQUS Euler-Bernoulli and 2-noded Timoshenko element

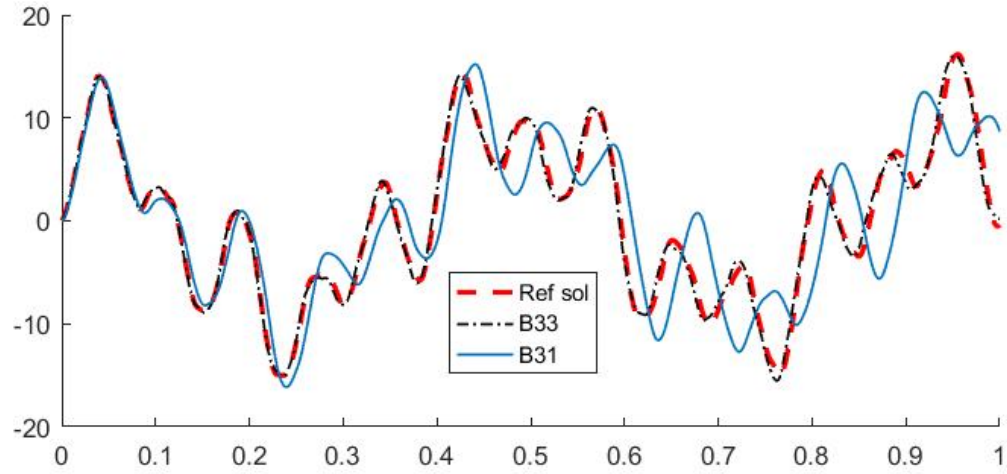

Figure 4.19: Velocity plot for the ABAQUS Euler-Bernoulli and 2-noded Timoshenko element

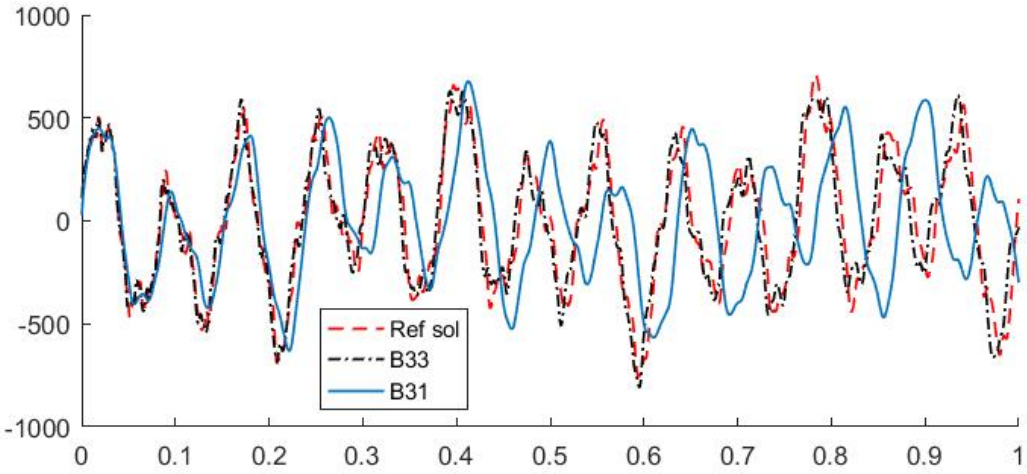

Figure 4.20: Acceleration plot for the ABAQUS Euler-Bernoulli and 2-noded Timoshenko element

The quadratic elements GEQ2 and B32 have been compared in Figure 4.21, 4.22 and 4.23. For the displacement, the two elements coincide perfectly with each other and the reference solution. Looking at the velocity plot in figure 4.22, the two solutions still coincide with each other, but no longer with the reference solution over the whole time domain. Looking at the acceleration plot, the two elements are still indistinguishable.

Comparing the velocity and acceleration plots of the quadratic GE element with the cubic GE element in Figure 4.24 and 4.25, the cubic element clearly comes out on top. The cubic element coincides with the reference solution for the velocity, and has a better approximation of the peaks in the acceleration plot.

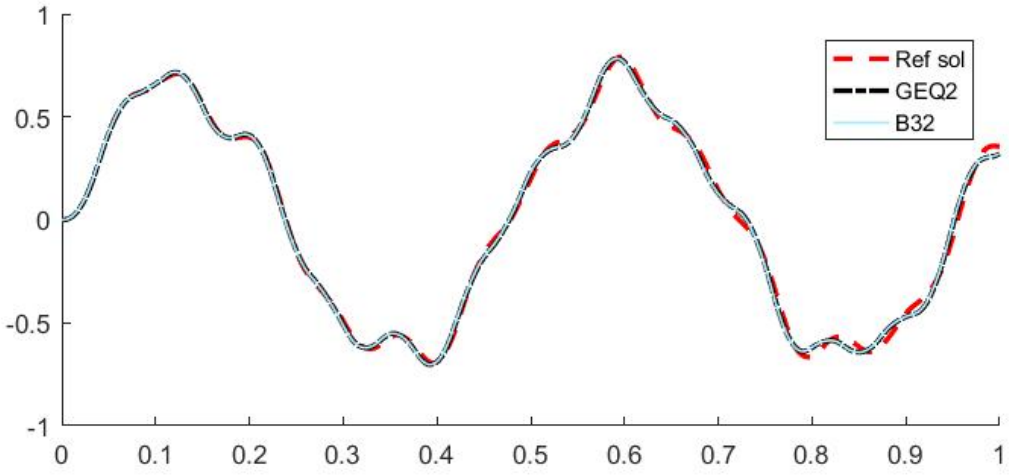

Figure 4.21: Displacement plot for the quadratic elements

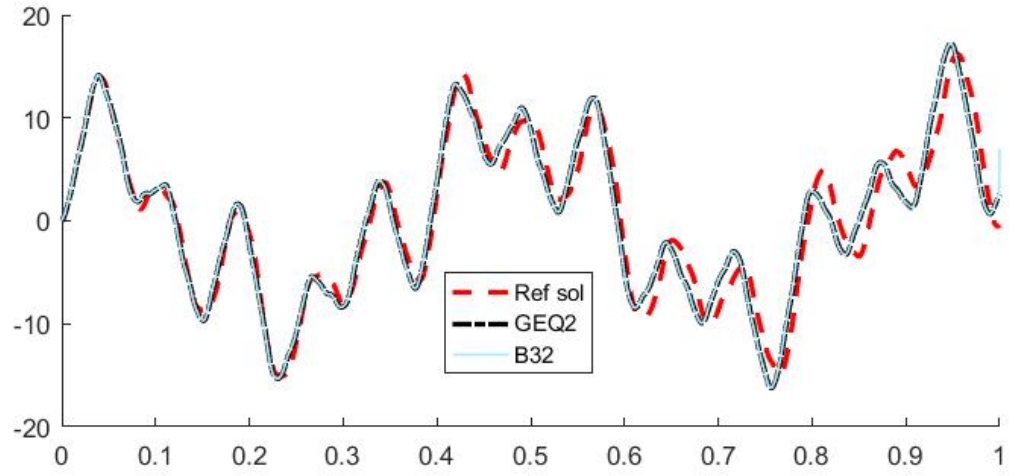

Figure 4.22: Velocity plot for the quadratic elements

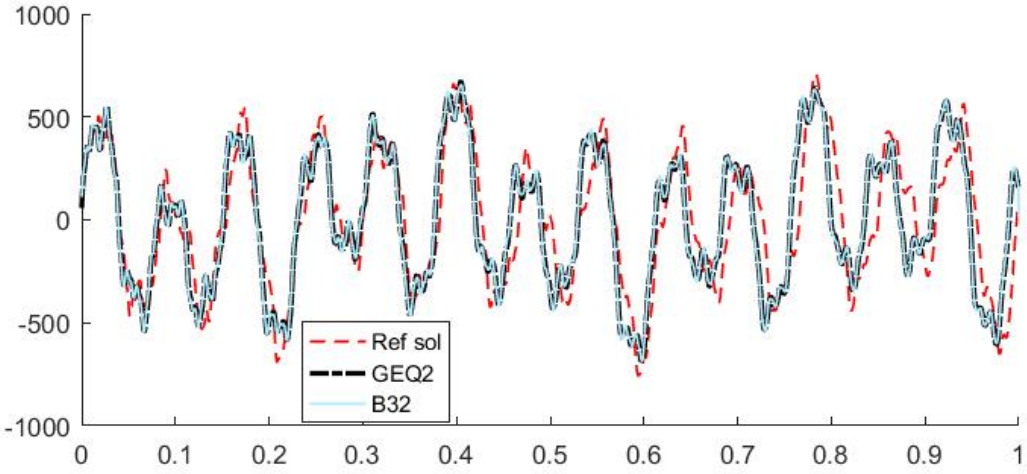

Figure 4.23: Acceleration plot for the quadratic elements

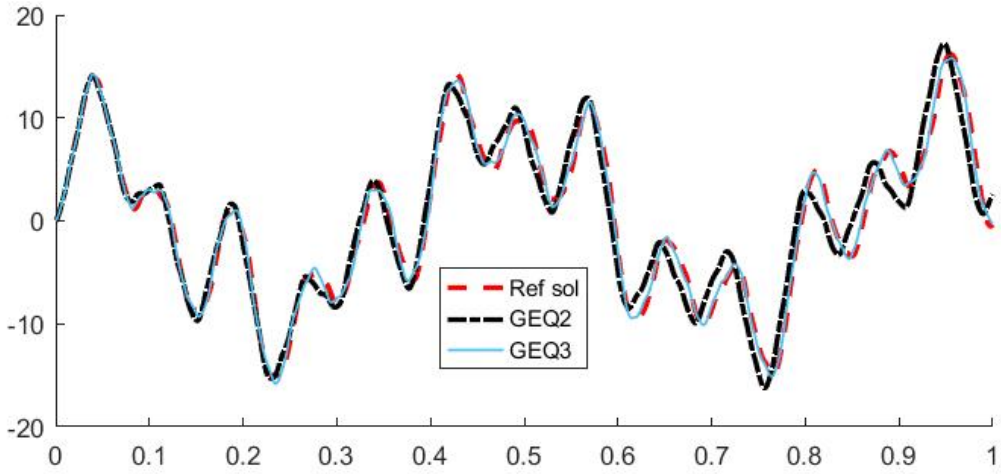

Figure 4.24: Velocity plot for the quadratic and cubic GE elements

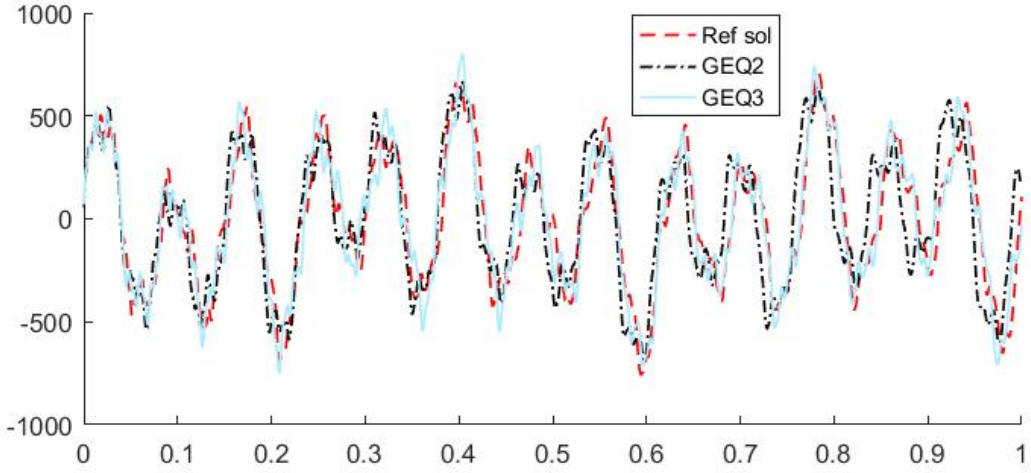

Figure 4.25: Acceleration plot for the quadratic and cubic GE elements

Chapter 5

Summary and Conclusion

In this master thesis a review of the geometrically exact (GE) beam model presented in [15] for static and dynamic analysis of beam-like 3D structural problems has been presented. In Chapter 2, the Timoshenko beam element[17] has been compared to the Euler-Bernoulli element. Chapter 2 also describes the shear locking phenomena and remedies to eliminate it. The solving of nonlinear equilibrium equations for static and dynamic problems has been described in Chapter 3, as well as the strain measures utilized by IFEM and ABAQUS. Chapter 4 presents the numerical results.

In this master thesis the GE beam element, an in-house software developed by SINTEF ICT, has been compared with the well known and highly regarded beam elements from ABAQUS. The problems solved in this thesis have large displacements and rotations, but small to moderate strains, making them ideal for comparing the two formulations. The numeric results shows that the higher order elements perform better both when it comes to accuracy and rate of convergence for all the problems, thus making them

attractive despite of their theoretical and numerical complexity. The results also shows that enhancing the 2-noded GE beam element with residual bending flexibility increases the performance. This is in accordance to the findings made by Kjell M. Mathisen et al.[15]. Further work should entail developing a GE corotational beam formulation.

Bibliography

[1] On Finite Deformations of Space-curved Beams. *J.Appl. Math. Phys.*, pages 734–744, 1981.

[2] Anna Bauer, Michael Breitenberger, B. Phillipp, Roland Wüchner, and K.U. Bletzinger. Nonlinear Spatial Bernoulli Beam. *Comput. Meth.Appl. Mech. Engrg*, pages 101–127, 2016.

[3] P. Betsch and P. Steinmann. Frame-indifferent beam finite elements based upon the geometrically exact beam theory. *Comput. Meth.Appl. Mech. Engrg*, pages 1775–1788, 2002.

[4] A. Cardona and M. Géradin. A Beam Finite Element Non-linear Theory with Finite Rotations. *Int. J. Numer. Meth. Engrg*, pages 2403–2438, 1988.

[5] M. A Consistent Corotational Formulation for Non-linear Three-dimensional Beam Elements Crisfield. A Beam Finite Element Non-linear Theory with Finite Rotations. *Comput. Meth.Appl. Mech. Engrg*, pages 131–150, 1990.

[6] T.J.R Hughes. *The Finite Element Method.* Prentice-Hall, 1987.

[7] Thanh-Nam Le. Nonlinear Dynamics of Flexible Structures Using Corotational Beam Elements. pages 10–13, 2013.

[8] R.H MacNeal. *Finite Elements: Their Design and Performance*. Marcel Dekker, 1994.

[9] Abaqus Analysis User's Manual. 25.3.3 choosing a beam element.

[10] Abaqus Analysis User's Manual. 3.5.2 beam element formulation.

[11] Abaqus Analysis User's Manual. 3.5.5 mass and inertia for timoshenko beams.

[12] Kjell M. Mathisen. Introduction to Nonlinear FEA, 2016.

[13] Kjell M. Mathisen. Solution of Nonlinear Dynamic Equilibrium Equations, 2016.

[14] Kjell M. Mathisen. Solution of Nonlinear Equilibrium Equations, 2016.

[15] Kjell M. Mathisen, Yuri Bazilevs, Bjørn Haugen, Tore A. Helgedagsrud, Trond Kvamsdal, Knut M. Okstad, and Siv B. Raknes. A Comparative Study of Beam Element Formulations for Nonlinear Analysis: Corotational vs Geometrically Exact Formulations. *Proceedings of 9th National Conference on Computational Mechanics (MekIT'17)*, 2017.

[16] opensees.berkeley.edu. Hilber-hughes-taylor method.

[17] Eugenio Oñate. Structural Analysis with the Finite Element Method. Linear Statics. Volume 2: Beams, Plates and Shells:37–58, 2013.

[18] Eugenio Oñate. Structural analysis with the finite element method. linear statics. Volume 2: Beams, Plates and Shells:1–10, 2013.

[19] Roland Wüchner, Michael Breitenberger, and Anna Bauer. Isogeometric Structural Analysis and Design. *Chair of Structural Analysis Technical University of Munich*, 2016.

A IFEM Input Files

Dynamic

<?xml version="1.0" encoding="UTF-8" standalone="yes"?>

<!– Basic 1D elastic beam test. Cantilever beam with tip load. !–>

<simulation>

<geometry L="10.0">
<refine patch="1" u="5"/>
<raiseorder patch="1" u="0"/>
<topologysets>
<set name="Fixed end" type="vertex">
<item patch="1">1</item>
</set>
<set name="All" type="curve">
<item patch="1"/>
</set>
<set name="Loaded end" type="vertex">
<item patch="1">2</item>

```
</set>
</topologysets>
</geometry>

<boundaryconditions>
<dirichlet set="Fixed end" comp="123456"/>
<dirichlet set="All" comp="246"/>
</boundaryconditions>

<beam type="Timoshenko">
<!–addRBF/!–>
<material E="210e9" nu="0.3" rho="7850"/>
<properties H="0.5" B="0.25"/>
<nodeload u="1.0" dof="3" type="expression"> P0=1000000.0;
omega=50.0;P0*sin(omega*t)
</nodeload>
</beam>

<discretization>
<nGauss>3</nGauss>
</discretization>

<linearsolver class="dense"/>

<newmarksolver alpha="-0.05" alpha1="0.0" alpha2="0.0" rotation="total"
```

```
initacc="true">
<rtol>1.0e-16</rtol>
<convnorm>energy</convnorm>
<trueinertia/>
<timestepping>
<step start="0.0" end="1.0">5.0e-4</step>
</timestepping>
</newmarksolver>

<postprocessing>
<resultpoints>
<point patch="1" u="0.0"/>
<point patch="1" u="1.0"/>
</resultpoints>
</postprocessing>

</simulation>
```

Three Legged Beam

<?xml version="1.0" encoding="UTF-8" standalone="yes"?>

<!– Basic 1D elastic beam test.

3-segment cantilever with slope discontinuities.

Clamped at one end (at 0,0,0) and a nodal load at the free end. !–>

<simulation>

<geometry>

<patchfile>beamXYZ.G2</patchfile>

<refine lowerpatch="1" upperpatch="3" u="127"/>

<raiseorder lowerpatch="1" upperpatch="3" u="0"/>

<topologysets>

<set name="root" type="vertex">

<item patch="1">1</item>

</set>

<set name="tip" type="vertex">

<item patch="3">2</item>

```
</set>
</topologysets>
</geometry>

<boundaryconditions>
<dirichlet set="root" comp="123456"/>
</boundaryconditions>

<beam type="Timoshenko">
<!–addRBF/!–>
<material E="1.0e6" G="5.0e5"/>
<properties B="0.1" H="0.1"/>
<nodeload patch="3" u="1" dof="1" type="linear">-10.0</nodeload>
<nodeload patch="3" u="1" dof="3" type="linear">-10.0</nodeload>
</beam>

<geometry>
<topology>
<connection master="1" mvert="2" slave="2" svert="1"/>
<connection master="2" mvert="2" slave="3" svert="1"/>
</topology>
</geometry>

<discretization>
<nGauss>3</nGauss>
```

```
</discretization>

<nonlinearsolver rotation="total">
<timestepping>
<step start="0.0" end="1.0">20</step>
</timestepping>
<rtol>1.0e-16</rtol>
<dtol>1.0e+05</dtol>
<noEnergy/>
</nonlinearsolver>

<postprocessing>
<resultpoints>
<point patch="3" u="1.0"/>
</resultpoints>
</postprocessing>

</simulation>
```

Curved Beam

```
<?xml version="1.0" encoding="UTF-8" standalone="yes"?>

<!– Basic 1D elastic beam test. Cantilever arc with tip shear load. !–>

<simulation>

<geometry>
<patchfile>arc45.g2</patchfile>
<refine patch="1" u="127"/>
<raiseorder patch="1" u="0"/>
<topologysets>
<set name="innspenning" type="vertex">
<item patch="1">1</item>
</set>
</topologysets>
</geometry>

<boundaryconditions>
```

```
<dirichlet set="innspenning" comp="123456"/>
</boundaryconditions>


    <beam type="Timoshenko">
<material E="1.0e7" G="5.0e6"/>
<properties B="1.0" H="1.0"/>
<nodeload u="1" dof="3" type="linear">600.0</nodeload>
</beam>

<discretization>
<nGauss>3</nGauss>
</discretization>

<nonlinearsolver rotation="total">
<timestepping>
<step start="0.0" end="1.0">0.1</step>
</timestepping>
<rtol>1.0e-16</rtol>
<dtol>1000.0</dtol>
<noEnergy/>
</nonlinearsolver>

<postprocessing>
<resultpoints>
<point patch="1" u="1.0"/>
```

</resultpoints>

</postprocessing>

</simulation>

B ABAQUS Input FIles

Dynamic

*Heading

** Job name: TestBeam Model name: Model-1

** Generated by: Abaqus/CAE 6.12-1

*Preprint, echo=NO, model=NO, history=NO, contact=NO

**

** PARTS

**

*Part, name=Part-1

*Node

1, 0., 0., 0.

7, 10., 0., 0.

*Element, type=B32

1, 1, 2, 3

*Ngen, nset=Set-1

1, 7, 1 *Elgen, elset=Set-1

1, 3, 2, 1

** Section: Section-1 Profile: Profile-1

*Beam General Section, elset=Set-1, density=7850., section=general,

poisson=0.3

1.25e-1, 6.5104167e-4, 0., 2.6041667e-3, 3.90625e-3

0., 1., 0.

2.1e+11, 6.730769232e10

*End Part

**

**

** ASSEMBLY

**

*Assembly, name=Assembly

**

*Instance, name=Part-1-1, part=Part-1

*End Instance

**

*Nset, nset=Set-1, instance=Part-1-1

1,

*Nset, nset=Set-2, instance=Part-1-1

7,

*End Assembly

**

** BOUNDARY CONDITIONS

**

** Name: BC-1 Type: Displacement/Rotation

*Boundary

Set-1, 1, 6

```
*Amplitude, name=sinewave, definition=periodic
1, 50, 0, 0
0, 1
**initial conditions,type=solution,user
** ----------------------------------------------------------------
**
** STEP: Step-2
**
*Step, name=Step-2, nlgeom=YES, inc=10000000, amplitude=ramp
*Dynamic,direct,nohaf,alpha=-0.05
0.0005, 1.0,
**
** LOADS
**
** Name: Load-2 Type: Concentrated force
*Cload, amplitude=sinewave
Set-2, 3, 1.e+6
**
** OUTPUT REQUESTS
**
*Restart, write, frequency=0
**
** FIELD OUTPUT: F-Output-1
**
*Output, field, frequency=1
```

```
*Node Output
U,
**
** HISTORY OUTPUT: H-Output-1
**
*Output, history, variable=PRESELECT, frequency=1
*Node Print, nset=Set-2
U3, V3, A3
**El print, elset=Part-1-1.Set-1
** nforc
*End Step
```

Three Legged Beam

*Preprint, echo=NO, model=YES, history=NO, contact=NO

*PART, NAME=PART-1

*NODE

1, 0, 0, 0

257, 1, 0, 0

515, 1, 1, 0

769, 1, 1, 1

*ELEMENT, TYPE=B32

1, 1, 2, 3

*ELEMENT, TYPE=B32

129, 257, 258, 259

*ELEMENT, TYPE=B32

257, 515, 516, 517

*NGEN, NSET=SET-1

1, 257, 1

*NGEN, NSET=SET-2

257, 515, 1

*NGEN, NSET=SET-3

515, 769, 1

*ELGEN, ELSET=SET-1

1, 128, 2, 1

*ELGEN, ELSET=SET-2

129, 128, 2, 1

*ELGEN, ELSET=SET-3

257, 128, 2, 1

*BEAM GENERAL SECTION, ELSET=SET-1, DENSITY=7850, SECTION=GENERAL, POISSON=0.0

0.0100000000, 0.0000083333, 0, 0.0000083333, 0.0000200000

0,1,0

1000000.0000000000, 416666.6666666667

*BEAM GENERAL SECTION, ELSET=SET-2, DENSITY=7850, SECTION=GENERAL, POISSON=0.0

0.0100000000, 0.0000083333, 0, 0.0000083333, 0.0000200000

-1,0,0

1000000.0000000000, 416666.6666666667

*BEAM GENERAL SECTION, ELSET=SET-3, DENSITY=7850, SECTION=GENERAL, POISSON=0.0

0.0100000000, 0.0000083333, 0, 0.0000083333, 0.0000200000

-1,0,0

1000000.0000000000, 416666.6666666667

*END PART

*ASSEMBLY, NAME=ASSEMBLY

*INSTANCE, NAME=PART-1-1, PART=PART-1

*END INSTANCE

*NSET, NSET=SET1, INSTANCE=PART-1-1

1,

*NSET, NSET=SET2, INSTANCE=PART-1-1

382,

*END ASSEMBLY

** CREATE BC

*BOUNDARY

SET1, ENCASTRE

*STEP, NAME=STEP$_BC, AMPLITUDE = RAMP, INC = 1000, NLGEOM = YES$

$* STATIC, DIRECT$

$1e-3, 1.0$

$* *$

$* CLOAD$

$SET2, 1, -10$

$SET2, 3, -10$

$* *$

$* CONTROLS, RESET$

$*CONTROLS, PARAMETERS = FIELD, FIELD = DISPLACEMENT$

$1e-04, 1e-07, , , , , ,$

$* CONTROLS, PARAMETERS = FIELD, FIELD = ROTATION$

$1e-04, 1e-07, , , , , ,$

$* RESTART, WRITE, FREQUENCY = 0$

$* *Requestdisplacementsandrotations$

$*OUTPUT, FIELD$

$*NODEOUTPUT, NSET = SET2$

U, UR

$**$

$*ENDSTEP$

Curved Beam

*Heading

** Job name: TestBeam Model name: Model-1

** Generated by: Abaqus/CAE 6.12-1

*Preprint, echo=YES, model=YES, history=NO, contact=NO

**

** PARTS

**

*Part, name=Part-1

*Node

1, 0., 0., 0.

9, 29.2893218813452, 70.7106781186547, 0.

10, 100., 0., 0.

*Element, type=B31

1, 1, 2

*Ngen, nset=Set-1, LINE=C

1, 9, 1, 10

*Elgen, elset=Set-1

1, 8, 1, 1

```
** Section: Section-1 Profile: Profile-1
*Beam General Section, elset=Set-1, density=7850., section=GENERAL,
poisson=0.0
1., 8.333333333333333e-2, 0., 8.333333333333333e-2, 1.7e-1
-1., 0., 0.
1.e+7, 4.901960785e+6
*End Part
**
**
** ASSEMBLY
**
*Assembly, name=Assembly
**
*Instance, name=Part-1-1, part=Part-1
*End Instance
**
*Nset, nset=Set-1, instance=Part-1-1
1,
*Nset, nset=Set-2, instance=Part-1-1
501,
*End Assembly
**Amplitude, name=sinewave, definition=periodic
** 1, 50., 0., 0.
** 0., 1.e+7
**
```

```
** BOUNDARY CONDITIONS
**
** Name: BC-1 Type: Displacement/Rotation
*Boundary
Set-1, ENCASTRE
**initial conditions,type=solution,user
** ———————————————————————————-
**
** STEP: Step-1
**
*Step, name=Step-1, nlgeom=YES, inc=1000000
*Static
.01, 1.0
**
** LOADS
**
** Name: Load-2 Type: Concentrated force
*Cload
Set-2, 3, 600.
**
** CONTROLS
**
*Controls, reset
*Controls, parameters=field, field=displacement
1e-06, 1e-09, , , , , ,
```

```
*Controls, parameters=field, field=rotation
1e-06, 1e-09, , , , , ,
**
** OUTPUT REQUESTS
**
*Restart, write, frequency=0
**
** FIELD OUTPUT: F-Output-1
**
*Output, field, frequency=1
*Node Output
U,
**
** HISTORY OUTPUT: H-Output-1
**
*Output, history, frequency=1
*Node Output, nset=Set-2
U,
*Node Print, nset=Set-2
U1,U2,U3,UR1,UR2,UR3
*El print, elset=Part-1-1.Set-1
nforc
*End Step
```